

# **Solar Wind Influence On The Oxygen Content of Ion Outflow In The High Altitude Polar Cap During Solar Minimum Conditions**

H. A. Elliott and R. H. Comfort  
The University of Alabama In Huntsville, Huntsville, Alabama

P. D. Craven and M. O. Chandler  
Space Science Laboratory, NASA Marshall Space Flight Center, Huntsville Alabama

T. E. Moore  
Laboratory for Extraterrestrial Physics, NASA Goddard Space Flight Center, Greenbelt,  
Maryland

## **Author Information**

Heather A. Elliott  
Space Science Directorate, Code SD50  
Marshall Space Flight Center  
Huntsville, AL 35812  
Phone: 256-544-3972  
Fax: 256-544-5244  
Email:Heather.Elliott@msfc.nasa.gov

Richard H. Comfort  
CSPAR  
The University of Alabama in Huntsville  
Huntsville, AL 35899  
Phone: 256-890-6663  
Fax: 256-890-6575  
Email:comfortr@cspar.uah.edu

Paul D. Craven  
Space Science Directorate, Code SD50  
Marshall Space Flight Center  
Huntsville, AL 35812  
Phone: 256-544-7639  
Fax: 256-544-5244  
Email:Paul.Craven@msfc.nasa.gov

Michael O. Chandler  
Space Science Directorate, Code SD50  
Marshall Space Flight Center  
Huntsville, AL 35812  
Phone: 256-544-7645  
Fax: 256-544-5244  
Email:Michael.Chandler@msfc.nasa.gov

Thomas E. Moore  
Interplanetary Physics Branch, Code 692  
Laboratory for Extraterrestrial Physics  
Goddard Space Flight Center  
Greenbelt, MD 20771  
Phone: 301-286-5236  
Fax: 301-286-1683  
Email:Thomas.E.Moore@gssc.nasa.gov

## Abstract

We correlate solar wind and IMF properties with the properties of O<sup>+</sup> and H<sup>+</sup> in the polar cap in early 1996 during solar minimum conditions at altitudes between 5.5 and 8.9 Re geocentric using the Thermal Ion Dynamics Experiment (TIDE) on the POLAR satellite. Throughout the high altitude polar cap, we observe H<sup>+</sup> to be more abundant than O<sup>+</sup>. Oxygen ions are of primary interest in this study because they are commonly used as a tracer of the ionospheric component. We observe O<sup>+</sup> to be most abundant at lower latitudes when the solar wind speed is low (and low K<sub>p</sub>), while at higher solar wind speeds (and high K<sub>p</sub>) O<sup>+</sup> is observed across most of the polar cap. We also find that O<sup>+</sup> density and parallel flux are well organized by solar wind dynamic pressure; they both increase with solar wind dynamic pressure. The O<sup>+</sup> density has a higher correlation with the solar wind dynamic pressure when IMF B<sub>z</sub> is positive than when IMF B<sub>z</sub> is negative. H<sup>+</sup> is not as highly correlated with solar wind and IMF parameters, but H<sup>+</sup> density and parallel flux are negatively correlated with IMF B<sub>y</sub>, and positively correlated with  $V_{sw} B_{IMF}$ . In this solar minimum data set, H<sup>+</sup> is dominant, so that contributions of this plasma to the plasma sheet would have very low O<sup>+</sup> to H<sup>+</sup> ratios.

## 1. Introduction

The high altitude (> 5.5Re) polar cap plasma is not a well known because it is often low in both density and energy which makes it difficult to observe. Only recently have the low energy ions of this plasma been studied with POLAR/TIDE ([Moore *et al.*, 1997; and Su *et al.*, 1998]. There are contributions to the magnetosphere from both the solar wind and ionosphere, and particles circulate within the magnetosphere. The overall circulation of the particles in the magnetosphere is not well known. Understanding what particles will pass through the high-

altitude polar cap is important to understanding the overall circulation because magnetic field lines connect this region to the magnetosheath and to the tail. In the high altitude polar cap, both H<sup>+</sup> and O<sup>+</sup> are flowing away from the Earth and have such low temperatures that they are thought to originate from the ionosphere [Moore *et al.*, 1997; and Su *et al.*, 1998], but it is not clear what the latitude or local time of the source is. Due to a combination of parallel flow and convection (which vary with IMF and solar wind conditions), ions at any given point in the polar cap could originate from different source regions such as the polar cap, cleft, or aurora. Changes in the IMF and solar wind can affect ionospheric outflows by changing the electric fields that convect ions as they flow outward, and by changing the shape of the field lines along which ions flow. Since the ions observed in this study are highly field-aligned, the second effect is likely to be very important. Not only is the part of the ionosphere which is the source not clear, but the destination of these ions is also not clear. These particles could become part of the magnetosheath or the plasma sheet.

Chappell *et al.* [1987] estimated that the ionospheric particle source is sufficient to supply the entire magnetospheric plasma content. The relative contributions of ionospheric and solar wind plasma to the plasma sheet population is still a controversial topic. Several studies have used trajectory models to understand the ionospheric contribution to the plasma sheet and ring current [Moore *et al.*, in press; Delcourt *et al.*, 1988; Sauvaud and Delcourt, 1987; Delcourt *et al.*, 1994; Delcourt *et al.*, 1989]. Additional studies by Abshour-Abdalla *et al.*, [1997 and 1999] use trajectory models to compare contributions from the solar wind and ionosphere. Their results showed the solar wind to be a more important source than the ionosphere to the plasma sheet. Pilipp and Morfill [1978] attributed plasma sheet formation to mantle plasma with their model.

Based on ion measurements of particle distributions, Eastman *et al.* [1984] put forth the concept that ionospheric ions enter the plasma sheet from the lobes via the plasma boundary layer. Borovsky *et al.* [1997] and Borovsky *et al.* [1998] have shown that the plasma sheet density is well correlated with the solar wind density. Based on that correlation they concluded that the plasma sheet is likely to be of solar wind origin. Lennartsson [1992] explained the plasma sheet being more solar-wind-like during northward IMF than southward IMF by having solar wind particles entering the plasma sheet along the flanks of the Low Latitude Boundary Layer (LLBL) during northward IMF. Recent work by Winglee *et al.* [1998] also shows differences in the plasma sheet for different IMF  $B_z$  conditions; for southward IMF the ionospheric source is more important to the plasma sheet, but for northward IMF the solar wind source is more important.

We use the unique ability of the Thermal Ion Dynamics Experiment (TIDE) and the Plasma Source Instrument (PSI) to measure the low energy plasma of the high altitude polar cap. Previous studies of TIDE data with PSI operating at Polar's apogee have focused on inter-comparing the properties of  $H^+$  ions to those of  $O^+$  and  $He^+$  [Su *et al.*, 1998; and Moore *et al.*, 1997]. This study goes further by relating the properties of outflowing ions to the solar wind and IMF conditions. Recent work by Winglee [1998] includes an ionospheric source as a low altitude boundary condition to his multi-fluid model of the magnetosphere. By keeping track of which particles were ionospheric particles and which were solar wind, Winglee showed that the ionospheric source is more important than the solar wind source to the plasma sheet for southward IMF conditions, and vice versa for northward IMF conditions. By providing ion measurements that are sorted by IMF and solar wind conditions, this study constrains magnetospheric models.

The IMF and solar wind can affect ionospheric outflows by changing the electric fields that convect ions across field lines as they flow outward, and by changing the shape of the field lines along which ions flow. Understanding the relationship of the IMF and solar wind to the properties of H<sup>+</sup> and O<sup>+</sup> ions in the polar cap may therefore give insight into which ionospheric source regions (cusp/cleft, aurora, and polar cap) are dominant. It is well known that in the ionosphere, anti-sunward convection in the polar cap is observed during southward IMF conditions, and sunward convection can occur for strong northward IMF intervals. In the northern hemisphere when IMF  $B_y$  is strongly positive and  $B_z$  is negative, the whole convection pattern is rotated from noon towards dawn, and vice versa for negative  $B_y$  [Burch *et al.*, 1985; Weimer, 1995; Weimer, 1996; Reiff and Burch, 1985; Lu *et al.*, 1989; Rich and Maynard, 1989; and Heppner and Maynard, 1987]. Several studies have found relationships between polar ion outflows and changing IMF conditions at lower altitudes than the data presented in this study [Waite *et al.*, 1986; Chandler *et al.*, 1995; Pollock *et al.*, 1990; Lockwood *et al.*, 1985b; and Delcourt *et al.*, 1988].

Ions flowing out of the ionosphere have been shown to disperse according to their mass and energy as they are swept away from the source by convection, the Geomagnetic Mass Spectrometer (GMS) effect. A persistent dayside source of upwelling ions was shown to exist by Lockwood *et al.* [1985a], and Moore *et al.* [1986] concluded that this dayside source of upwelling ions was collocated with the cleft. Waite *et al.*, [1986] showed a connection between the IMF and geomagnetic activity levels with the outflows from the cleft that form a GMS. Their results showed that O<sup>+</sup> flows out of the cleft region and then falls into the middle of the polar

cap for low  $K_p$ , but flows further tailward for high  $K_p$ . In that same paper, they also found that the IMF affected the motion of  $O^+$  ions by controlling the convection pattern. For  $B_y$  negative conditions they observed more  $O^+$  in the dusk region than in the dawn region, and they concluded that the ions are convected duskward from the source region in the cleft. For  $B_y$  positive, ions were convected more towards dawn. Chandler *et al.* [1995] showed that  $O^+$  on average flows out of the dayside and falls into the nightside polar cap when  $B_z < 0$ , but on average for  $B_z > 0$   $O^+$  flows out of the entire polar cap. The upwelling ion source latitude in the cleft was shown to depend on  $B_z$  by Pollock *et al.* [1990] and Lockwood *et al.* [1985], but the occurrence frequency of upwelling ions and the intensity did not depend on  $B_z$  [Pollock *et al.*, 1990].

In addition to the data studies mentioned above, simulations have also found relationships between the IMF and ion outflow. A simulation study by Delcourt *et al.* [1988] examines the effects of different IMF conditions on the trajectories of low energy ions. They modeled ions flowing out of the nightside polar cap using two different convection patterns; a two cell pattern, indicative of southward IMF conditions, and a four cell pattern, indicative of northward IMF conditions. Their results show that the latitude at which ions are started, the ion mass, and the convection pattern greatly affect the trajectories. When a two cell convection pattern is used,  $O^+$  ions starting in the middle of the polar cap do not pass through the plasma sheet more than 5  $R_e$  downtail. However,  $O^+$  ions starting at the same location for a four cell convection pattern go much farther into the plasma sheet, while  $H^+$  ions started at the same location go tailward and towards the magnetosheath for a four cell pattern. Delcourt *et al.* [1988] attribute the difference in  $H^+$  and  $O^+$  destinations to  $O^+$  having a smaller parallel velocity.  $O^+$  ends up in a different part of the convection pattern due to its lower parallel velocity. This causes  $O^+$  to gain energy as

it passes through a region of negative electric field azimuthal component (in spherical coordinates) because the energy gain is proportional to the azimuthal electric field.

Even the ionospheric source region has been shown to depend on the IMF,  $K_p$ , and the local convection speed. Loranc *et al.* [1991] showed that vertical upflows in the polar ionosphere occur mostly in the cusp and auroral region where horizontal convection is the largest, and downflows are most probable in the polar cap. For southward IMF conditions, upflows are mostly in the cusp and auroral regions, but the downflows are mostly inside the polar cap [Loranc *et al.*, 1991]. For northward IMF, they showed that both upflows and downflows occur in the polar cap.

$O^+$  is of particular interest due to its large mass, which requires more energy to escape than  $H^+$ . Classical polar wind models predict that only  $H^+$  and  $He^+$  will escape. Even though  $O^+$  has a large mass and typically has energies less than 1keV in the lower polar magnetosphere, Geotail measurements have shown the presence of cold  $O^+$  beams in the mid-tail lobe/mantle region [Mukai *et al.*, 1994], and deep in the tail lobe/mantle region [Hirahara *et al.*, 1997 and Seki *et al.* 1996]. It is also widely known that  $O^+$  in the inner magnetotail and plasma sheet has a definite dependence on magnetic activity [e.g. Daglis and Axford, 1996; and Lennartsson and Shelley, 1986].

The acceleration of heavy species has been linked in several studies to strong convection and convection reversals in the cusp cleft region. Lockwood *et al.* [1985b] and Horwitz and Lockwood [1985] showed that for strong convection,  $O^+$  is spread from the cleft across the

entire polar cap at altitudes between 1.5 and 4 Re. It is likely that the distance at which O<sup>+</sup> is spread across the polar cap by convection also correlates with other solar wind and IMF parameters because the solar wind causes the applied electric field, and the convection pattern is controlled by the IMF orientation via reconnection effects. Su *et al.* [1998] concluded that at 5000 km altitude the most likely source region for O<sup>+</sup> thermal ions is the cleft/cusp, a region of high solar wind and magnetospheric interaction. According to case studies of the cleft ion fountain by Wilson and Craven [1999], molecular outflows from the cleft are associated with regions of strong convection in the cusp. Broadband electrostatic noise and strong field-aligned currents were also observed when the strong cusp convection was observed [Wilson and Craven, 1999]. Pollock *et al.* [1990], Moore *et al.* [1986], and Lockwood *et al.* [1985a] also noted that upwellings are associated with convection reversals and currents in the cleft. In summary, the articles discussed above show a connection between outflows and convection; and the convection pattern and IMF.

This paper first briefly describes the TIDE and PSI instruments and the data set used, along with the solar wind data, and the method of solar wind propagation. An average picture of the H<sup>+</sup> and O<sup>+</sup> properties in the polar cap as a function of latitude is presented for the entire data set, and as a function of invariant latitude for high and low solar wind speeds. In the remaining parts of the paper, direct correlations between solar wind and IMF parameters and H<sup>+</sup> and O<sup>+</sup> parameters are discussed. The last two sections focus on the relationship between O<sup>+</sup> properties and the solar wind dynamic pressure and  $V_{sw}B_{IMF}$ ; and the relationship between H<sup>+</sup> and O<sup>+</sup> properties and IMF  $B_y$ .

## 2. Experimental Approach

This section describes the TIDE Instrument, the way in which the TIDE data was reduced, how comparisons were made with solar wind and IMF data, and the scope of the data set. The primary instrument used in this study is TIDE, and details about this instrument have been given by Moore *et al.* [1995]. Mass is distinguished on TIDE using a carbon foil time-of-flight system, and energy is determined using a Retarding Potential Analyzer (RPA) and an electrostatic mirror. The energy range is from the spacecraft potential to 450 eV. Although TIDE is capable of measuring 3-D ion phase space distribution functions in 6 seconds, in the high altitude polar cap, integrations of at least 1 minute are required to improve the signal-to-noise ratio. Solar wind data are available on a time resolution of about 1.6 minutes, so this is the time resolution used for this study. By performing numerical integrations of moments of the TIDE ion distribution function in velocity space, the density, velocity, and temperature of the ions are determined. TIDE is able to observe plasma in the high altitude magnetospheric polar cap by operating in conjunction with the Plasma Source Instrument (PSI), a plasma contactor [Comfort *et al.*, 1998; and Moore *et al.*, 1995], that reduces the electric potential on the spacecraft from tens of volts to about 2.0 volts. The average spacecraft potential in the polar cap at apogee without PSI operating is about 25 V which is enough to shield out nearly all of the H<sup>+</sup> ions, and a significant fraction of the O<sup>+</sup> ions. We could study some of the O<sup>+</sup> without PSI operating, but then the data set would be biased towards times when the O<sup>+</sup> energy is high.

The data set used in this study is limited for several reasons. One reason is that 3-D measurements of the velocity distribution with mass resolution are only available from April to July of 1996, during solar minimum conditions. This data set is limited further to times when PSI

is operating so this low energy and low density plasma of the high altitude polar cap can be examined. There were only ten passes with PSI operating when 3-D measurements were obtained at apogee. For one of those passes, the WIND satellite was not in the solar wind so IMP 8 data were used for that pass. The magnetic field measurements are obtained from the Magnetic Field Instrument (MFI) on WIND and from the magnetometer (MAG) on IMP 8, and the particle measurements are obtained from the Solar Wind Experiment (SWE) on Wind and from the plasma instrument (PLA) on IMP 8.

Since solar wind and IMF measurements are made at large distances upstream from the magnetosphere in the solar wind, it is necessary to estimate the time it takes for the solar wind to reach the magnetosphere before attempting to correlate solar wind data with magnetospheric data. The method of propagating IMF measurements is based primarily on the work of Ridley *et al.* [1998], and references therein. In this study the magnetopause has been chosen as the common reference point for solar wind and IMF data. The magnetopause position has been estimated by balancing the solar wind dynamic pressure and magnetic pressure of the magnetosphere. Ridley *et al.* [1998] tested four different methods of calculating the propagation delay time by comparing the calculated delay to the actual delay between the measurement of a dramatic change in either the Y or Z component at WIND and the measurement of that same change at IMP8. Our study uses the X distance only method since it is much simpler and is nearly as accurate as the best method. Ridley *et al.* [1998] estimate that the error in delay times calculated using the X-distance only method is ( $\pm$ ) 8.6 min. An additional delay has been added to account for a delay for passage through the magnetosheath, and this delay was also calculated as in Ridley *et al.* [1998].

After having shifted the solar wind data, the polar cap H<sup>+</sup> and O<sup>+</sup> density, parallel velocity, parallel flux, dynamic pressure, and perpendicular velocity are correlated with solar wind and IMF parameters and combinations of these parameters. Many pairs of parameters have been correlated, but the results presented in this paper focus on the strongest correlations found. In addition to the solar wind parameters, we also present average K<sub>p</sub> values for each orbit pass for reference.

We tried to determine if there was an additional delay for travel times of ions from the ionospheric source to the high altitude magnetospheric polar cap. We varied the delay time from -10 min to 3 hours in 1 minute steps and then recalculated the correlation coefficients at each step for several pairings of TIDE versus solar wind/IMF quantities. We chose pairs that we found to correlated well with O<sup>+</sup> and H<sup>+</sup> with no additional delay. This process was done for 3 passes two that had high solar wind speed and two that had low solar wind speed. We chose these passes because they represented the extremes in conditions. This process did not turn out to be helpful. We found pairs that correlated well when using the entire data set did not always correlate well when examining individual passes. For example, no one pass correlated well with the solar wind dynamic pressure, but when all the passes were combined a correlation was observed between O<sup>+</sup> density and the solar wind dynamic pressure. The variation of the correlation coefficient for a given pair of quantities versus delay time varied drastically from pass to pass. Each pair of quantities that we correlated had a different response curve. Since no clear additional delay time could be found, we have not included any such delay.

Many general features of H<sup>+</sup> ions are apparent in the spin and energy spectrograms shown in Figures 1 and 2 respectively. These figures show that in spin (Figure 1) H<sup>+</sup> is usually a narrow beam field aligned beam, but occasionally it is observed over a wide range of angles. Although not shown in these examples, the field aligned beams sometimes cover a wider range of spin angles. Plasma velocity distributions included in this study are all flowing out away from the Earth, and have energies within TIDE's energy range. The examples in Figures 2 show that the H<sup>+</sup> energy flux varies significantly in energy, and there are times within the polar cap where TIDE clearly does not measure the peak energy of the distribution. One example of this is on 05/28/96 when the IMF was northward (Figure 2). Examination of HYDRA key parameter data shows the presence of energetic electrons and ions which are likely to be associated with an auroral arc. Even though we show these intervals on the spectrograms to show the overall polar cap structure, such intervals are not included in this study. No downward flowing O<sup>+</sup> or H<sup>+</sup> is observed in our data set. Either there are no downflowing O<sup>+</sup> or H<sup>+</sup> at this altitude, or the fluxes are too low to be detected by TIDE. It could be possible for us to observe mantle ions that have precipitated and then reflected such that they flow out away from the Earth [Moore *et al.*, 1999a; Rosenbauer *et al.*, 1975; and Shelley *et al.*, 1976]. Our energy criterion may not have eliminated all mantle ions because some mantle ions have been observed to have energies that lie within TIDE's energy range [Newell *et al.*, 1991; and Moore *et al.*, 1999a]. However, the orbit plots show that most of the data in this study lies on the nightside, and mantle ions are more likely to be found on the dayside. Unlike H<sup>+</sup>, O<sup>+</sup> is usually a cold field-aligned beam as shown in Figure 3.

Figure 4 shows the Polar satellite orbital segments in magnetic local time (MLT) and invariant (INVLAT) when TIDE and PSI are both operating. Figure 5a shows all the subintervals in which the distribution of H<sup>+</sup> is observed entirely within TIDE's energy range. This energy range criterion limits this data set to primarily the nightside. In Figure 5a and b, the density is color coded. Figure 5b shows the portions of the orbits where O<sup>+</sup> was observed. Note that O<sup>+</sup> density is much lower than the H<sup>+</sup> density. Times when the H<sup>+</sup> densities are high, do not always correspond to times when the O<sup>+</sup> densities are high. We generally observe H<sup>+</sup> throughout the polar cap although there are brief intervals where none is observed (Figures 1 and 2). A low level of O<sup>+</sup> flux is often detected along the field line (Figure 3), but the intervals where we detected no O<sup>+</sup> are longer than the intervals when we detected no H<sup>+</sup>.

### **3. O<sup>+</sup> and H<sup>+</sup> Latitudinal Structure At High and Low $V_{sw}$**

Table 1 contains the corresponding average solar wind speeds for the passes shown in the spin-time spectrograms of O<sup>+</sup> in Figure 3. The two passes on 04/19/96 are ones in which the solar wind speeds and the O<sup>+</sup> fluxes are the largest. In Table 1 we also show the corresponding Kp averages for each orbital pass and the daily Kp averages. From this table it can be seen that Kp is higher on the passes where the solar wind speed is higher. Since the Kp and the solar wind speed are both high, it is difficult to distinguish which is more important. Although the solar wind speed and Kp were high on the two 04/19/96 passes, the solar wind dynamic pressure was not high. The first pass on 04/19/96 had a dynamic pressure of 3.5 nPa and the second had a dynamic pressure of 2.5 nPa. A typical value of the solar wind dynamic pressure is 2.6 nPa. In the other passes, the larger fluxes are mostly observed in or near the cusp and aurora.

Figure 6 shows all of the O<sup>+</sup> TIDE density, velocity, and flux measurements averaged into 2 degree invariant latitude bins, and shows the same type of curves for high ( $V_{sw} > 500\text{km/s}$ ) and low solar wind speeds ( $V_{sw} < 500\text{ km/s}$ ) in a different line style. The sample distribution is also shown for reference (Figure 6d). The latitudinal profiles for low solar wind speeds are very similar to those for the entire data set since most of the data is at low to moderate solar wind speeds. At low solar wind speeds the density decreases with increasing latitude (Figure 6a), but the velocity is nearly constant (Figure 6b), so that the parallel flux (Figure 6c) also decreases with increasing latitude. The average density is a factor of two larger at high solar wind speed compared to low solar wind speeds, and the parallel speed is about the same so the parallel flux is also a factor of two larger. The density and parallel flux are more uniform in latitude at high solar wind speeds. Figure 7 shows the same type of data for H<sup>+</sup> as is shown for O<sup>+</sup> in Figure 6. The H<sup>+</sup> average density (Figure 7a) is more than an order of magnitude larger than the O<sup>+</sup> density, and the H<sup>+</sup> average parallel velocity (Figure 7b) is twice the O<sup>+</sup> average velocity. The parallel flux (Figure 7c) and parallel velocity (Figure 7b) are fairly uniform with latitude. Although the parallel velocity looks like it may be greater at high and low latitudes, this is not significant given the size of the standard deviation at those latitudes. The average values of the H<sup>+</sup> parameters at high solar wind speeds differ only slightly from the averages for the entire data set as show in Figure 7, but the profiles differ. The H<sup>+</sup> parallel velocity increases with latitude. A different profile in H<sup>+</sup> density is also observed at high solar wind speeds; the density decreases instead of being constant as it is at low solar wind speeds.

Perpendicular velocity (convection drift) has been determined using both H<sup>+</sup> and O<sup>+</sup> measurements (Figure 8). The average H<sup>+</sup> perpendicular speed is about 4 km/s larger than the

O+ average perpendicular speed (Figure 8a), although the O+ curve lies within the standard deviation of the H+ curve. A small difference in the average direction is also observed. The angle shown here in Figure 8b is defined as the arctangent of  $V_y \text{ GSM}/V_x \text{ GSM}$ , so zero degrees is sunward and 90 degrees is duskward. Our measurements show that the polar cap convection for this data is on average anti-sunward.

For many of the passes, the counts for O+ are very low. The H+ raw count rates are usually an order of magnitude greater and hence have a much lower error. All the moments are sums of the distribution function over energy, azimuth angle, and polar angle. Since the distribution function is derived from the count rate, there is a corresponding error term. Individual passes have been examined and the passes that have the largest disagreement in convection velocity are those in which the O+ counts are the lowest.

#### 4. Direct Correlations With IMF and Solar Wind

Next we examine direct correlations with the solar wind and IMF properties. Correlation coefficients used in this study are Pearson linear correlation coefficients ( $R$ ). To evaluate how large a correlation coefficient must be to be meaningful with real data, a significance level is determined. This study uses a level derived by Borovsky *et al.* [1998]. They defined a confidence interval for the correlation coefficient at the 95% confidence level in the same manner as Bendat and Piersol [1971]. The value of  $r$  for which there is no correlation at the 95% confidence level is then  $R \leq \frac{2}{\sqrt{N}}$  [Borovsky *et al.*, 1998]. Correlation coefficients in this study are presented along with the ratio of the correlation coefficient to  $\frac{2}{\sqrt{N}}$  which in this paper this

ratio is called Rcl. Borovsky *et al.* [1998] considers any  $Rcl \leq 1.6$  to be a weak correlation. In this paper we conclude that a linear correlation is only meaningful when  $Rcl \geq 1.6$ .

#### 4.1. O+ Correlation With Solar Wind Dynamic Pressure and $V_{sw}B_{sw}$

Although the O+ density correlates well with both the dynamic pressure and with  $V_{sw}B_{IMF}$ , it has a higher correlation with the solar wind dynamic pressure. Parallel flux, on the other hand, correlates better with  $V_{sw}B_{IMF}$ . Figure 9a shows the relationship between the log of the solar wind dynamic pressure, and the log of the O+ density in the polar cap for the entire data set. For the entire data set the correlation coefficient is 0.532 without averaging the data into bins, and is 0.950 when a bin size of 0.02 is used (Figure 9b). Figures 9c and d are similar to Figure 9b except that the data have been sorted according to the sign of IMF Bz. Throughout the remainder of the paper, the correlation coefficient obtained using the data without being binned will follow in parentheses the correlation coefficient obtained using the binned data. The correlation coefficient between the solar wind dynamic pressure and the O+ density is larger when IMF Bz is northward (Figure 9c), and the slope for northward IMF is steeper than for southward IMF (Figure 9d). For northward IMF Bz the correlation coefficient between the O+ density and the dynamic pressure (0.955(0.624)) is greater than for southward IMF Bz (0.894(0.470)). The parallel flux does not correlate as well with the dynamic pressure (Figure 10) as the density does because the parallel velocity does not correlate well with the solar wind dynamic pressure.

Density is not as well correlated with  $V_{sw}B_{IMF}$  as the parallel flux; the density has a coefficient of 0.865(0.516) (Figure 11a), while the parallel flux has correlation of 0.896(0.611) (Figure 11b).

The positive correlation between the parallel velocity and  $V_{sw}B_{IMF}$  ( $R=0.244$ ) leads to a slightly better correlation between  $V_{sw}B_{IMF}$  and the parallel flux than between  $V_{sw}B_{IMF}$  and density. The solar wind dynamic pressure and  $V_{sw}B_{IMF}$  are related quantities and hence are highly correlated with each other ( $0.926(0.720)$ ). The solar wind speed has a correlation coefficient of  $0.701(0.495)$  with the density, but those data are not presented here because there was no measured speeds between 405 km/s and 620 km/s.

## 4.2. H+ and O+ Correlation With IMF By

In general, H+ is not correlated as well with IMF and solar wind parameters as is O+. The H+ density and parallel flux correlate best with IMF By and  $V_{sw}B_{IMF}$ . The H+ density is anticorrelated with IMF By, as shown in Figure 12a, with a correlation coefficient of  $-0.829(-0.43)$ . This negative correlation is stronger when IMF By is negative.

The H+ flux does not correlate as well with IMF By (Figure 12b) as the density because the velocity has a slight positive correlation. Parallel speed does not correlate as well as the density does with IMF and solar wind parameters for either H+ or O+ (Figure 13a and b). For both species, the parallel speed correlated better with IMF By than any other solar wind or IMF parameters. Each species has a very different relationship between its parallel speed and IMF By; the H+ parallel velocity increases with IMF By and the O+ parallel velocity decreases. The O+ density has a different relationship with IMF By than H+. O+ density and parallel flux have a nonlinear relationship with IMF By (Figures 14a and b).

The O+ density and H+ density were also examined as a function of MLT and INVLAT. The largest H+ densities are observed on the dusk side when IMF By is negative, although our coverage is limited and more data is needed to determine if this relationship is significant. When IMF By is positive, no clear dawn-dusk asymmetry in the H+ density is observed. No clear dawn-dusk asymmetry is apparent in the O+ density for either sign of IMF By. This study can be extended substantially by using the data that is not mass discriminated, but since H+ and O+ seem to have different relationships with IMF By, such a study would give ambiguous results.

### 4.3. H+ Correlation With VswBsw

The H+ density has a dependence on  $V_{sw}B_{IMF}$ ; the correlation coefficient between the two is 0.667(0.328) (Figure 15a). Figure 15b shows that there is also a correlation between the parallel flux and  $V_{sw}B_{IMF}$  is 0.756(0.354). When IMF Bz is positive, the correlation coefficient between the H+ parallel flux and  $V_{sw}B_{IMF}$  is smaller 0.5151(0.321) (Figure 15c) than when the IMF is southward (Figure 15d), and the correlation coefficient is 0.827(0.434).

## 5. Discussion

In this study we have tried to determine under what conditions O+ is plentiful. O+ is observed most of the time, but can be at very low flux levels. Higher fluxes are observed when the solar wind speed is high and when the spacecraft is near the polar cap boundary. O+ densities and parallel flux have high linear correlations with the solar wind dynamic pressure,  $V_{sw}B_{IMF}$ , and the solar wind speed. The cases that have higher solar wind speeds also have higher Kp, so that the O+ density also shows a correlation with Kp. These correlations provide insight regarding the

source region and have implications for circulation. The differences between H<sup>+</sup> and O<sup>+</sup> also are important for identifying the source.

The H<sup>+</sup> density in general did not correlate as well with solar wind and IMF parameters as O<sup>+</sup> did, but it did show some negative correlation with IMF B<sub>y</sub> and a positive correlation with  $V_{sw} B_{IMF}$ . O<sup>+</sup> did not have a linear response like H<sup>+</sup> with IMF B<sub>y</sub>, rather it had a more complex non-linear response. Not only did H<sup>+</sup> have lower correlation coefficients with the solar wind and IMF parameters, but it was also more abundant than O<sup>+</sup> for the solar minimum conditions in this data set. H<sup>+</sup> outflows are a persistent feature and are not as dependent on the geophysical conditions. Classical models predict that H<sup>+</sup> can readily escape due to its light mass, but predict that O<sup>+</sup> is gravitationally bound. The large mass of O<sup>+</sup> means that its escape energy is larger. Since more energy is available during more active times, it is more likely for the amount of O<sup>+</sup> observed in the high altitude polar cap during active times to be larger. O<sup>+</sup> ions being more plentiful in the polar cap during active times is not surprising since O<sup>+</sup> ions have been shown to be more abundant during active times elsewhere in the magnetosphere in particular the ring current and inner plasma sheet. It is important to note that the O<sup>+</sup> to H<sup>+</sup> density ratio of the ion outflow changes with geophysical conditions. Chappell *et al.* [1987] discusses this, and they point out that an increasing O<sup>+</sup> to H<sup>+</sup> ratio in the plasma sheet may represent a change in the ion outflow composition, not a change in the importance of the ionospheric source relative to the importance of the solar wind source.

Results of other studies are consistent with the relationships found in our study. Most of the studies have examined outflows found in the polar cap at lower altitudes. Only one case study

by Moore *et al.* [1999a] has examined outflows in relationship to IMF and solar wind parameters in the altitude range found in our study. Moore *et al.* [1999a] showed a possible connection between the properties of the solar wind speed and dynamic pressure and O<sup>+</sup> outflows at high altitudes. They examined the polar cap response to a Coronal Mass Ejection (CME) and found that subsequent to the CME impact, large fluxes of O<sup>+</sup> were observed. The pressure and solar wind speed were both large after the CME passage. The solar wind speed was greater than 800km/s and the solar wind dynamic pressure was 12-15 nPa. The polar cap O<sup>+</sup> ions were so energetic at one point they moved out of the TIDE energy range and into the TIMAS energy range. Our correlations are consistent with their case study in that we observe more O<sup>+</sup> at higher solar wind speeds and dynamic pressures. Moore *et al.* [1999a] also analyzed O<sup>+</sup> measurements at low altitudes (5000 km) where it was shown that O<sup>+</sup> fluxes correlated best with the hourly standard deviation of the solar wind dynamic pressure. In our study the solar wind dynamic pressure did not vary much. The two passes that had the largest amounts of O<sup>+</sup> did not have much variation in the dynamic pressure, but they did have high solar wind speeds and moderate solar wind dynamic pressures (Most of our data was at low solar wind speed and dynamic pressures.). Our results at high altitudes show a linear correlation with the solar wind dynamic pressure that the Moore *et al.* [1999a] results did not show at lower altitudes. Our results also show a possible correlation with solar wind speed, but our coverage in solar wind speed was not adequate to determine a linear fit.

O<sup>+</sup> and H<sup>+</sup> not having the same relationships with IMF and solar wind parameters could suggest that O<sup>+</sup> and H<sup>+</sup> come from different source regions or that their paths differ due to their different masses. Su *et al.* [1998] concluded that at lower altitudes (5000 km), most of the O<sup>+</sup> comes from

the cleft. The cleft/cusp region is a region where the solar wind interacts more strongly with magnetosphere. If O<sup>+</sup> comes from the cleft/cusp region and H<sup>+</sup> does not, then that might explain why O<sup>+</sup> correlates more strongly than H<sup>+</sup> with the solar wind dynamic pressure,  $V_{sw}B_{IMF}$ , and the solar wind speed. The work of Giles [1993] also indicates that O<sup>+</sup> beams at altitudes greater than 3 Re originate as asymmetric distributions (cleft upwelling signature). Her data and model results indicated that the asymmetric distributions evolve into conics and then beams as they flow to higher altitudes. She also examined the occurrence frequency of O<sup>+</sup> asymmetric distributions. She found that at higher solar wind dynamic pressures and solar wind speeds the asymmetric O<sup>+</sup> distribution occurrence frequencies were larger. She showed that the occurrence frequencies of O<sup>+</sup> asymmetric distributions were lower for IMF B<sub>z</sub> negative than for IMF B<sub>z</sub> positive, but that those same occurrence frequencies were slightly larger for K<sub>p</sub> >3 than for K<sub>p</sub> <3. We observe more O<sup>+</sup> at high K<sub>p</sub>, and the O<sup>+</sup> density versus solar wind dynamic pressure relationship has a larger correlation and a steeper slope for IMF B<sub>z</sub> positive. Giles [1993] also showed that both the O<sup>+</sup> asymmetric distributions at altitudes less than 3Re and the O<sup>+</sup> field aligned beams at altitudes greater than 3 Re were more abundant when  $-VXB$  was larger. Since we find that the O<sup>+</sup> beam density and flux correlates well with the solar wind speed, the solar wind dynamic pressure,  $VB$ , and K<sub>p</sub> which is similar to correlations found by Giles [1993] for asymmetric distributions in the cleft upwelling region, we believe that the source of these O<sup>+</sup> beams is the cleft. This statement is also supported by the Giles [1993] finding that O<sup>+</sup> asymmetric distributions evolve into O<sup>+</sup> beams at higher altitudes.

Su [1998] also examined also compared the H<sup>+</sup>, O<sup>+</sup>, and He<sup>+</sup> velocity ratios to those predicted by different processes such as velocity filter, centrifugal acceleration, electrostatic acceleration,

and gravitational force. She concluded that the  $V_{O^+} : V_{He^+} : V_{H^+}$  ratio spanned all the possibilities, but that equal energy gain possibly due to an electrostatic potential layer came the closest to representing the average state. The flaw in using such ratios is that if all species do not have the same source or if different sources are active at different times then comparing the average velocity ratios from data obtained at different times may give inconclusive results. Su examined the  $O^+$  density as a function of  $X$  in SM coordinates and found that  $O^+$  was variable across the polar cap with some downward trend and concluded that  $O^+$  could at times be from the cleft ion fountain. We went further and examined more passes and sorted by geophysical conditions. This turned out to be useful in comparing with the cleft ion fountain model work by Horwitz and Lockwood [1985] and Lockwood *et al.* [1985b].

Model results also provide information that leads us to conclude that the  $O^+$  we observe at 8.9  $R_E$  geocentric originates in the cleft. Horwitz and Lockwood [1985] simulated  $O^+$  outflow in the cleft ion fountain and showed that for low convection speeds. The  $O^+$  parallel energy was greatest near the cleft and drops off sharply in the polar cap. At high convection speeds the  $O^+$  parallel energy dropped off less sharply such that significantly larger parallel energies were found in the polar cap. They observed that the density dropped off significantly with altitude for both high and low convection, and that  $O^+$  was spread further into the polar cap in the high convection case. The differences they observed for high and low convection speeds are due to higher convection speeds moving  $O^+$  further away from the source. Lockwood *et al.* [1985b] used  $K_p$  as a proxy for high and low convection speeds to compare data with the model results of Horwitz and Lockwood [1985] at high and low convection speeds. They showed that at high  $K_p$   $O^+$  was observed further from the cleft, but at low  $K_p$  it was confined to regions near the cleft.

Horwitz and Lockwood [1985] parallel energy results at 5 Re geocentric are qualitatively similar to our results. We observe the parallel speed to be constant with latitude at low Kp and Vsw, but at high Kp and Vsw we observe the parallel speed to increase with increasing latitude. From their figure (Figure 4a [Horwitz and Lockwood, 1985]), it appears that the same gradients in parallel energy occurs at altitudes greater than those in their model. It is more difficult for us to compare with their density contour maps because the contours are so sparse at higher altitudes, although we do observe more O+ in the nightside polar cap for our high Kp and Vsw cases.

No significant IMF Bz dependence was found with either O+ or H+ measurements in our study. This is surprising since models of O+ cleft ion outflow show a dependence on the antisunward polar cap flows which is determined primarily by the IMF Bz [eg. Horwitz and Lockwood, 1985]. Chandler *et al.*, [1995] showed that, on average, for IMF Bz negative, O+ flows mainly upwards on the dayside and downwards on the nightside. For IMF Bz positive, their results showed that O+ flow is mainly upwards. IMF Bz seemed to have the largest effect on the downflows in the Chandler *et al.* [1995] study since upflows occur independent of the sign of IMF Bz. At the altitudes observed in our study, both H+ and O+ are outflowing even for IMF Bz < 0, so we would not necessarily expect to find an IMF Bz effect. A study by Lockwood *et al.* [1990] of the drivers of convection also provides insight about possible IMF Bz effects. Lockwood *et al.* [1990] concluded that high-latitude polar cap convection is generated by direct solar wind control on the dayside, and from reconnection in the tail on the nightside. A nightside response to a change in IMF Bz could be delayed from the direct dayside response. The convection response to IMF Bz is complex in the middle of the polar cap because both the

nightside and dayside have equal influences [Lockwood *et al.*, 1990]. We may not obtain a good correlation with IMF Bz by combining our data because the response of convection (which affects ion outflow trajectory) to changes in IMF Bz is so complex. Therefore, case study analysis seems more appropriate for examining IMF Bz effects.

Lockwood *et al.* [1990] also predict that IMF By should change the dawn-dusk asymmetry in the convection pattern within 10-15 minutes. According to Lockwood *et al.* [1990] direct solar wind driven convection is most effective on newly open lines in the merging region because the magnetic field changes rapidly in time on newly open field lines, which causes the curl of the electric field to be large. On field lines that have been open for an extended period, the further stretching of the field lines does not produce a large electric field. The convection in the polar cap is then driven by newly opened flux at the merging site, and is not due to mapping of field lines from the ionosphere-magnetosphere directly into the magnetosheath. So changes in convection due to changing IMF By, which affects the tension at the merging site, would affect the whole convection pattern. IMF By does not have competing day and nightside effects like IMF Bz does. The IMF By correlation that we observe in our H<sup>+</sup> and O<sup>+</sup> data could be because the convection pattern is controlled by IMF By or the overall magnetospheric magnetic field line configuration is IMF By dependent.

Delcourt *et al.* [1988] showed that the convection pattern determines where H<sup>+</sup> and O<sup>+</sup> end up in the tail. Since O<sup>+</sup> has a larger mass, its parallel velocity is lower, causing it to follow a different path, and possibly be energized by a different amount. In the Delcourt *et al.*, [1988] study, O<sup>+</sup> drifted further away from the midnight meridian in the eastward direction. For a southward IMF

2-cell convection pattern they predict that both O<sup>+</sup> and H<sup>+</sup> will end up in the plasma sheet, but at different distances downtail. For a northward IMF 4-cell convection pattern, they predict that O<sup>+</sup> will end up in the plasma sheet, but H<sup>+</sup> will head tailward and towards the magnetosheath. We found no IMF B<sub>z</sub> effect in our data when all the cases were combined; however, when case studies were examined we found qualitatively similar results to Delcourt *et al.* [1998]. On the second 04/19/96 pass our data shows antisunward polar cap convection (mostly southward IMF), and on 05/28/96 sunward flows (northward IMF) are observed [Moore *et al.*, 1999b]. Although no IMF B<sub>z</sub> effect was found when the data from each orbital pass were combined to form one large data set, we did find an IMF B<sub>y</sub> effect when analyzing the entire data set. In general IMF B<sub>y</sub> seems to be more important than IMF B<sub>z</sub> in affecting the H<sup>+</sup> and O<sup>+</sup> densities. Similar differences in O<sup>+</sup> and H<sup>+</sup> trajectories for different signs of IMF B<sub>z</sub> found by Delcourt *et al.* [1988], may occur in the H<sup>+</sup> and O<sup>+</sup> trajectories for different IMF B<sub>y</sub> conditions. Changes in the IMF B<sub>y</sub> have been linked to changes in the convection pattern, and as Delcourt *et al.* [1988] showed the azimuthal convection electric field is related to the amount of energization an ion can receive. In particular, O<sup>+</sup> may be affected more by the differences in the dawn-dusk convection for IMF B<sub>y</sub> positive or negative. A given flux tube O<sup>+</sup> and H<sup>+</sup> may have different amounts of O<sup>+</sup> and H<sup>+</sup> because the two species followed different paths.

IMF B<sub>y</sub> effects have also been found in data obtained at lower altitudes. Waite *et al.* [1986] found that at lower altitudes (1.11-4.65 Re) the O<sup>+</sup> occurrence frequency had an IMF B<sub>y</sub> dependence. They found that more O<sup>+</sup> was observed on the dusk side for IMF B<sub>y</sub> negative, and more O<sup>+</sup> was found on the dawn side for IMF B<sub>y</sub> positive. Waite *et al.* [1986] found that the asymmetry in the occurrence frequency matched the asymmetry in the convection pattern. We found no clear

asymmetry in our O<sup>+</sup> for IMF B<sub>y</sub> positive and negative or for H<sup>+</sup> for IMF B<sub>y</sub> positive. We did find that for IMF B<sub>y</sub> negative we observed more H<sup>+</sup> on the dusk side although our sample is not large enough to determine if this is generally the case. Our results in Figure 14s show that the O<sup>+</sup> density has a negative linear correlation at low magnitudes of IMF B<sub>y</sub>. H<sup>+</sup> density has a stronger negative linear correlation with IMF B<sub>y</sub> when IMF B<sub>y</sub> was negative, as shown in Figure 15.

Timing is also an important issue because some responses in the high altitude polar cap may be due to instantaneous changes in the magnetic field configuration and convection velocity, and others may be due to changes at the source region. If the source region is the ionosphere, a delayed response would be observed at 8 Re altitude. It could take O<sup>+</sup> anywhere from 45 min to 2 hours to go from the topside ionosphere to 8Re altitude. There has not been much work on modeling the response time of polar outflows [Schunk, 1999], and not many data studies either. Schunk [1999] analyzed the response times of both H<sup>+</sup> and O<sup>+</sup> to a geomagnetic storm. The maximum altitude examined in that study was 4000 km. His results show that H<sup>+</sup> responded immediately at 4000 km, and that O<sup>+</sup> began to respond 30 minutes later. Moore *et al.* [1999a] examined a Polar apogee pass with PSI operating that occurred right when a CME hit the magnetosphere. Based on changes in the particle spectrum they concluded that the whole configuration of the polar region changed drastically and immediately. Before the CME arrived, Polar was in the polar cap; and then immediately after the CME hit, Polar was in the mantle and eventually passed through the mantle and back into the polar cap several hours later, where a large amount of O<sup>+</sup> was observed. Some changes could be observed instantaneously because the shape and size of the magnetosphere respond immediately, causing a relatively stationary

satellite to suddenly be on different field lines when a solar wind driver changes. Daglis and Axford [1996] show that there is a fast and effective feeding of the inner magnetotail with ionospheric-origin ions during the expansion and the late growth phase of substorms. They show that energetic O<sup>+</sup> in the inner magnetotail has a sharp increase in energy density within 10 minutes of onset. Any immediate response of the polar cap lobe field lines is of interest because the plasma already on those field lines may convect down to the plasma sheet. A response to changes in the solar wind and IMF could occur at any altitude along a given flux tube. The only response does not have to be at the source region in the ionosphere. In this study we attempted to determine if there were delayed responses of both H<sup>+</sup> and O<sup>+</sup> by shifting the solar wind and IMF data by different time intervals and recalculating the correlation coefficients. We found no common delay time(s) for either H<sup>+</sup> or O<sup>+</sup>. Each pass had a different response curve for each pair of quantities correlated. Based on our results and the work of Baker [1986], studies of response time are better suited for case study analysis.

We did not find any significant correlations with solar wind density and H<sup>+</sup> or O<sup>+</sup> density. This is important because Borovsky *et al.* [1998] found that the plasma sheet density correlated with the solar wind density. We did find a similar correlation to the one found by Lennartsson and Shelley [1986] and references therein in the plasma sheet. They found that in the plasma sheet the O<sup>+</sup> to H<sup>+</sup> ratio increased with increasing AE. We found that the O<sup>+</sup> to H<sup>+</sup> ratio increases with increasing K<sub>p</sub>.

## 6. Summary and Conclusions

O<sup>+</sup> density correlated best with the solar wind dynamic pressure, solar wind speed, VB, and K<sub>p</sub>. At lower solar wind speeds, O<sup>+</sup> density decreased with increasing latitude, but this trend was not observed at higher solar wind speeds. On average the O<sup>+</sup> density is 0.025 cm<sup>-3</sup>, the average velocity is 23.2 km/s, and the average O<sup>+</sup> parallel flux is 5.25X10<sup>4</sup> cm<sup>-2</sup>s<sup>-1</sup>. At solar wind speeds greater than 500 km/s, the average velocity is about the same (22.5 km/s) as for the entire data set, but the density and parallel flux are larger (0.054 cm<sup>-3</sup> and 1.11X10<sup>5</sup> cm<sup>-2</sup>s<sup>-1</sup>). A nonlinear correlation was also observed between the O<sup>+</sup> density and IMF B<sub>y</sub>. Giles [1993] showed that the O<sup>+</sup> asymmetric distributions had higher occurrence frequencies when the solar wind dynamic pressure, solar wind speed, and -V<sub>XB</sub> were large. We conclude that the O<sup>+</sup> beams we observe at a higher altitude originate as asymmetric distributions at a lower altitude in the cleft region because the beams we observe have a similar correlation with the solar wind dynamic pressure and speed. Also, Giles [1993] concluded based on her data and model results that the asymmetric distributions observed at less than 3 Re probably evolved into beams at altitudes greater than 3 Re. At lower altitudes in the polar cap O<sup>+</sup> is thought to be primarily of cleft ion fountain origin. Su *et al.* [1998] arrived at the conclusion that most of the polar cap O<sup>+</sup> was from the cleft at 5000km altitude based on the downward motion of O<sup>+</sup> and the decreasing density from day to night. So it is not unreasonable that O<sup>+</sup> found at higher altitudes would also come from the cleft. Our results show a similar K<sub>p</sub> dependence as is predicted by the cleft ion fountain model work by Lockwood et al [1985b] and Horwitz and Lockwood [1985].

H<sup>+</sup> did not correlate as well as O<sup>+</sup> with solar wind and IMF parameters. H<sup>+</sup> density correlated best with, IMF B<sub>y</sub> and V<sub>B</sub>. Not only did H<sup>+</sup> have lower correlation coefficients with the solar wind and IMF parameters, but it was also more abundant than O<sup>+</sup> during the solar minimum conditions found in this data set. The average H<sup>+</sup> density, velocity, and parallel flux are all higher than those of O<sup>+</sup>; the average values are 0.45 cm<sup>-3</sup>, 42.8 km/s, and 1.76X10<sup>6</sup> cm<sup>-2</sup>s<sup>-1</sup>. The average values for H<sup>+</sup> at high solar wind speeds are about the same as those for those at low solar wind speeds. H<sup>+</sup> outflows are a persistent feature and are not as dependent on the geophysical conditions, and even classical polar wind models have no problem getting H<sup>+</sup> to escape due to its low mass. We conclude that H<sup>+</sup> could have several different source regions, or at different times different source regions are active. Both of these situations could make correlations difficult to determine when the data set consists of several passes with various geophysical conditions.

The large mass of O<sup>+</sup> means that its escape energy is larger, and since more energy is available during more active times, it is more likely for the amount of O<sup>+</sup> observed in the high altitude polar cap during active times to be larger. The relationships between IMF B<sub>y</sub> and both O<sup>+</sup> and H<sup>+</sup> densities could be related to the IMF B<sub>y</sub> control of convection and configuration of the magnetic field lines. A similar IMF B<sub>y</sub> effect was observed at lower altitudes by Waite *et al.* [1988]. Since O<sup>+</sup> and H<sup>+</sup> correlated differently with the IMF and solar wind, they probably have different sources

There have been some studies that examined the response of O<sup>+</sup> outflow in relation to K<sub>p</sub>, solar wind dynamic pressure, and IMF at lower altitudes, but there has been only one case study of O<sup>+</sup>

or  $H^+$  at these altitudes found in our study. At lower altitudes there have not been many studies of  $H^+$  in relationship to IMF or solar wind parameters because  $H^+$  is usually in part shielded by the spacecraft potential. Often  $H^+$  ion distributions are filled in to estimate the missing part of the distribution [Su *et al.*, 1998]. There are no indications that we are missing part of the  $H^+$  distribution at high altitudes because the  $H^+$  beam energy is larger at these altitudes. We observe no bite outs in the distributions at the spacecraft potential energy as is observed at lower altitudes. As Schunk [1999] pointed out, there have been few model studies of the outflow response timing either. In our epoch analysis we found no common delay time due to changes in the IMF or solar wind that would account for the transient time from the ionosphere to the magnetosphere. We conclude that delay time is best analyzed on a case by case basis. Fluid models of the magnetosphere are just beginning to incorporate ionospheric outflows into their models which are driven by the solar wind and IMF [ e.g. Winglee *et al.*, 1998]. We have provided new information about a region that is not well known. Perhaps with the inclusion of ion outflow in magnetospheric models with constraints added by observations, the fate of ionospheric ions will be determined. We have, in this study, provided data that will contribute to the models and to constrain them.

## **7. Acknowledgements**

We would like to thank the entire TIDE team for helpful discussions and development of group analysis tools. This project has been funded by the Alabama Space Grant Consortium from NASA Training Grant NGT5-40018 and by ISPA, the NASA – The University of Alabama In Huntsville cooperative agreement NCC8-65.

## References

- Abshour-Abdalla, M., M. El-Alaoui, V. Perroomian, R. J. Walker, J. Raeder, R. J. Walker, R. L. Richard, L. M. Zelenyi, L. A. Frank, W. R. Paterson, J. M. Bosqued, R. P. Lepoint, K. Ogilvie, S. Kokubun, T. Yamamoto, Ion sources and acceleration mechanisms inferred from local ion distributions, *Geophys., Res. Lett.*, *24* (8), pp. 955-958, 1997.
- Abshour-Abdalla, M., M. El-Alaoui, V. Perroomian, R. J. Walker, J. Raider, L. A. Frank, and W. R. Paterson, Source distributions of substorm ions observed in the near-Earth magnetotail, *Geophys., Res. Lett.*, *26* (97), pp. 955-958, 1999.
- Baker, D. N., Statistical analysis in the study of solar wind-magnetosphere coupling, *Solar Wind-Magnetosphere Coupling*, edited by Y. Kamide and J. A. Slavin, Terra Scientific Publishing Co., Dordrecht, pp. 17-38, 1986.
- Bendat, J. S., and A. G. Piersol, *Random Data: Analysis and Measurement Procedures*, John Wiley, New York, section 4, 1971.
- Borovsky, J. E., M. F. Thomsen, and R. C. Elphic, The superdense plasma sheet: Plasmaspheric origin, solar wind origin, or ionospheric origin, *J. Geophys. Res.*, *102* (A10), pp. 22,089-22,097, 1997.
- Borovsky, J. E., M. F. Thomsen, and R. C. Elphic, The driving of the plasma sheet by the solar wind, *J. Geophys. Res.*, *103* (A8), pp. 17,617-17,639, 1998.
- Burch, J. L., P. H. Reiff, J. D. Menietti, R. A. Heelis, W. B. Hanson, S. D. Shawhan, E. G. Shelley, M. Sugiura, D. R. Weimer, and J. D. Winningham, IMF By-dependent plasma flow and Birkeland currents in the dayside magnetosphere: 1. Dynamics Explorer Observations, *J. Geophys. Res.*, *90* (A2), pp.1577-1593, 1985.

- Chappell, C. R., T. E. Moore, and J. H. Waite, Jr., The ionosphere as a fully adequate source of plasma for the Earth's magnetosphere, *J. Geophys. Res.*, *92* (A6), pp. 5896-5910, 1987.
- Chandler, M. O., Observations of downward moving O<sup>+</sup> in the polar topside ionosphere, *J. Geophys. Res.*, *100* (A4), pp. 5795-5800, 1995.
- Comfort, R.H., T.E. Moore, P.D.Craven, C.J. Pollock, F.S. Mozer, and W.T. Williamson, Spacecraft potential control by on the POLAR satellite, *J. Spacecraft and Rockets*, *35* (6), pp. 845-849, 1998.
- Daglis, I. A., and W. I. Axford, Fast ionospheric response to enhanced activity in geospace: Ion feeding of the inner magnetotail, *J. Geophys. Res.*, *101* (A3), pp. 5047-5065, 1996.
- Delcourt, D. C., J. L. Horwitz, and K. R. Swinney, Influence of the interplanetary magnetic field orientation on polar cap ion trajectories: Energy gain and drift effects, *J. Geophys. Res.*, *93* (A7), pp. 7565-7570, 1988.
- Delcourt, D. C., C. R. Chappell, T. E. Moore, and J. H. Waite Jr., A three-dimensional numerical model of ionospheric plasma in the magnetosphere, *J. Geophys. Res.*, *94* (A9), pp. 11,893-11,920, 1989.
- Delcourt, D. C., T. E. Moore, and C. R. Chappell, Contribution of low-energy ionospheric protons to the plasma sheet, *J. Geophys. Res.*, *99* (A4), pp. 5681-5689, 1994.
- Eastman, T. E., L. A. Frank, W. K. Peterson, and W. Lennartsson, The plasma sheet boundary layer, *J. Geophys. Res.*, *89* (A3), pp. 1553-1572, 1984.
- Giles, B. L., *Inner magnetosphere circulation of thermal ions inferred from observed pitch angle distributions*, Ph.D. thesis, University of Alabama In Huntsville, Huntsville AL, 1993.
- Heppner, J. P., and N. C. Maynard, Empirical high-latitude electrical field models, *J. Geophys. Res.*, *92* (A5), pp. 4467-4489, 1987.

- Hirahara, M., T. Terasawa, T. Mukai, M. Hoshino, Y. Saito, S. Machida, T. Yamamoto, S. Kokubun, Cold ion streams consisting of double proton populations and singly charged oxygen observed at the distant magnetopause by Geotail: A case study, *J. Geophys. Res.*, *102* (A2), pp. 2359-2372, 1997.
- Horwitz, J. L., and M. Lockwood, The clef ion fountain: A two-dimensional kinetic model, *J. Geophys. Res.* *90* (A10), pp. 9749-9762, 1985.
- Lennartsson, W., A scenario for solar wind penetration of the Earth's magnetic tail based on ion composition data from the ISEE 1 spacecraft, *J. Geophys. Res.*, *97* (A12), pp. 19,221-19,238, 1992.
- Lennartsson, W., and E. G. Shelley, Survey of 0.1 to 16 keV/e plasma sheet ion composition, *J. Geophys. Res.*, *91* (A3), pp. 3061-3076, 1986.
- Lockwood, M., J. H. Waite, Jr., T. E. Moore, J. F. E. Johnson, and C. R. Chappell, A new source of suprathermal O<sup>+</sup> ions near the dayside polar cap boundary, *J. Geophys. Res.*, *90* (A5), pp. 4099-4116, 1985a.
- Lockwood, M., M. O. Chandler, J. L. Horwitz, J. H. Waite Jr., T. E. Moore, and C. R. Chappell, The cleft ion fountain, *J. Geophys. Res.*, *90* (A10), pp. 9736-9748, 1985b.
- Lockwood, M., S. W. H. Cowley, and M. P. Freeman, The excitation of plasma convection in the high-latitude ionosphere, *J. Geophys. Res.*, *95* (A6), pp. 7961-7972, 1990.
- Loranc, M., W. B. Hanson, R. A. Heelis, and J.-P. St. Maurice, A study of vertical ionospheric flows in the high-latitude F region, *J. Geophys. Res.*, *96* (A3), pp. 3627-3646, 1991.
- Lu, G., P. H. Reiff, M. R. Hariston, R. A. Heelis, and J. L. Karty, Distribution of convection potential around the polar cap boundary as a function of the interplanetary magnetic field, *J. Geophys. Res.*, *94* (A10), pp. 13,447-13,461, 1989.

- Moore, T. E., M. Lockwood, M. O. Chandler, J. H. Waite Jr., C. R. Chappell, A. Persoon, and M. Sugiura, Upwelling O<sup>+</sup> ion source characteristics, *J. Geophys. Res.*, *91* (A6), pp. 7019-7031, 1986.
- Moore, T. E., C. R. Chappell, M. O. Chandler, S. A. Fields, C. J. Pollock, D. L. Reasoner, D. T. Young, J. L. Burch, N. Eaker, J. H. Waite, Jr., D. J. McComas, J. E. Nordholdt, M. F. Thomsen, J. J. Berthelier, R. Robson, The Thermal Ion Dynamics Experiment, and Plasma Source Instrument., *Space Sci. Rev.*, *71*, pp. 409-458, 1995.
- Moore, T. E., C. R. Chappell, M. O. Chandler, P. D. Craven, B. L. Giles, C. J. Pollock, J. L. Burch, D. T. Young, J. H. Waite Jr., J. E. Nordhold, M. F. Thomsen, D. J. McCormas, J. J. Berthelier, W. S. Williamson, R. Robson, and F. S. Mozer, High-altitude observations of the polar wind, *Science*, *277*, pp. 349-351, 1997.
- Moore, T. E., W. K. Peterson, C. T. Russell, M. O. Chandler, M. R. Collier, H. L. Collin, P.D. Craven, R. Fitzenreiter, B. L. Giles, and C. J. Pollock, Ionospheric mass ejection in response to a CME, *Geophys. Res. Lett.*, *26* (15), pp. 2339-2342, 1999a.
- Moore, T. E., M. O. Chandler, C. R. Chappell, R. H. Comfort, P. D. Craven, D. C. Delcourt, H. A. Elliott, B. L. Giles, J. L. Horwitz, C. J. Pollock, and Y.-J. Su, Polar/TIDE results on polar ion outflows, *Sun-Earth Plasma Connections Geophysical Monograph 109*, Edited by J. L. Burch, R. L. Carovillano, and S. K. Antiochos, AGU, Washington, D.C., pp. 87-101, 1999b.
- Moore, T. E., B. L. Giles, D. C. Delcourt, and M.-C. Fok, The plasma sheet source groove, *J. Atmos. Solar Terr. Phys.*, in press, 1999c.
- Mukai, T., M. Hirahara, S. Machida, Y. Saito, T. Terasawa, and A. Nishida, Geotail

- observation of cold ion streams in the medium distance magnetotail lobe in the course of a substorm, *Geophys. Res. Lett.*, 21 (11), pp. 1023-1026, 1994.
- Newell, P. T., W. J. Burke, C.-I. Meng, E. R. Sanchez, and M. E. Greenspan, Identification and observations of the plasma mantle at low altitude, *J. Geophys. Res.*, 96 (A1), pp. 35-45, 1991.
- Pilipp, W., and G. Morfill, The formation of the plasma sheet resulting from plasma mantle dynamics, *J. Geophys. Res.*, 83, (A12), Pg. 5670-5678, 1978.
- Pollock, C. J., M. O. Chandler, T. E. Moore, J. H. Waite, Jr., C. R. Chappell, and D. A. Gurnett, A survey of upwelling ion event characteristics, *J. Geophys. Res.*, 95 (A11), pp. 18,969-18,980, 1990.
- Reiff, P. H., and J. L. Burch, IMF By-dependent plasma flow and Birkeland currents in the dayside magnetosphere: 2. A global model for northward and southward IMF, *J. Geophys. Res.*, 90 (A2), pp. 1595-1609, 1985.
- Rich, F. J., and N. C. Maynard, Consequences of using simple analytical functions for the high-latitude convection electric field, *J. Geophys. Res.*, 94 (A4), pp. 3687-3701, 1989.
- Ridley, A. J., G. Lu, C. R. Clauer, and V. O. Papitashvili, A statistical study of the ionospheric convection response to changing interplanetary magnetic field conditions using the assimilative mapping of ionospheric electrodynamics technique, *J. Geophys. Res.*, 103 (A3), pp. 4023-4039, 1998.
- Rosenbauer, H., H. Grünwaldt, M. D. Montgomery, G. Paschmann, and N. Sckopke, Heos 2 plasma observations in the distant polar magnetosphere: The plasma mantle, *J. Geophys. Res.*, 80 (19), pp. 2723-2737, 1975.
- Sauvaud, J. A., and D. C. Delcourt, A numerical study of suprathermal ionospheric ion

- trajectories in three-dimensional electric and magnetic field models, *J. Geophys. Res.*, *92* (A6), pp. 5873-5884, 1987.
- Seki, K., M. Hirahara, T. Terasawa, I. Shinohara, T. Mukai, Y. Saito, S. Machida, T. Yamamoto, S. Kokubun, Coexistence of Earth-origin O<sup>+</sup> and solar wind-origin H<sup>+</sup>/He<sup>++</sup> in the distant magnetotail, *Geophys. Res. Lett.*, *23* (9), pp. 985-988, 1996.
- Schunk, R. W., Ionospheric Outflow, *Sun-Earth Plasma Connections: Geophysical Monograph 109*, Edited by J. L. Burch, R. L. Carovillano, and S. K. Antiochos, AGU, Washington, D.C., pp. 195-206, 1999.
- Shelley, E. G., R. D. Sharp, and R. G. Johnson, He<sup>++</sup> and H<sup>+</sup> flux measurements in the day side cusp: Estimates of convection electric field, *J. Geophys. Res.*, *81* (12), pp. 2363-2370, 1976.
- Su, Y.-J., J. L. Horwitz, T. E. Moore, B. L. Giles, M. O. Chandler, P. D. Craven, M. Hirahara, and C. J. Pollock, Polar wind survey with Thermal Ion Dynamics Experiment/Plasma Source Instrument suite aboard POLAR, *J. Geophys. Res.*, *103* (A12), pp. 29,305-29,337, 1998.
- Waite, J. H. Jr., M. Lockwood, T. E. Moore, M. O. Chandler, J. L. Horwitz, and C. R. Chappell, Solar Wind Control of the Geomagnetic Mass Spectrometer, *Solar Wind-Magnetosphere Coupling*, Ed. Y. Kamide, J. A. Slavin, Terra Scientific Publishing Co., Dordrecht, pp. 707-716, 1986.
- Weimer, D. R., Models of high-latitude electric potential derived with a least error fit of spherical harmonic coefficients, *J. Geophys. Res.*, *100* (A10), pp. 19,595-19,607, 1995.
- Weimer, D. R., A flexible, IMF dependent model of high-latitude electric potentials having "space weather" applications, *Geophys. Res. Lett.*, *23* (18), pp.

2549-2552, 1996.

Wilson G. R. and P. D. Craven, Molecular ion outflow in the cleft ion fountain, *J. Geophys.*

*Res.*, *104* (A3), pp. 4437-4446, 1999.

Winglee, R. M., Multi-fluid simulations of the magnetosphere: The identification of the

geopause and its variation with IMF, *Geophys. Res. Lett.*, *25* (24), pp.

4441-4444, 1998.

## Figure Legends

**Figure 1.** Spin spectrograms of H<sup>+</sup> for two Polar satellite passes one on 04/19/96 (top) when the solar wind speed was high, and one on 05/28/96 (bottom) when the solar wind speed was low. Color scale indicates the energy flux. The spin angle of the spacecraft is on the y-axis. (X) is the ram direction, (+) is along the magnetic field and (-) is antiparallel to the magnetic field. The x-axis is UT time, and the MLT and invariant latitude of the spacecraft are also listed. The date of each pass is above each panel on the left side. The bars across the tops of the spectrograms indicate the instrument status where black is corresponds to operational, and gray means the mirror voltage settings have been adjusted which in this case means the instrument is turned off. The red stripe in the top figure corresponds to a time when TIDE was not operating.

**Figure 2.** H<sup>+</sup> energy spectrograms for passes on 04/19/96 (top) and 05/28/96 (bottom). This figure is different from Figure 1 in that the y-axis is the ion energy, and not the spin angle.

**Figure 3.** O<sup>+</sup> spin spectrograms with the same format as Figure 1.

**Figure 4.** Orbit of the POLAR satellite where the radius is invariant latitude and the angle is the magnetic local time when PSI and TIDE were operating at high latitudes during early 1996.

**Figure 5.** Orbit plots with the format the same format as Figure 4, but now the orbits are color coded according to the measured density. (a) shows the orbital segments where H<sup>+</sup> is present and meets the constraints of this study likewise (b) shows the same for O<sup>+</sup>. Note H<sup>+</sup> and O<sup>+</sup> have different color scales.

**Figure 6.** O<sup>+</sup> density (a), parallel velocity (b), parallel flux (c), and the number of samples as a function of invariant latitude. Here the data has been placed into latitude bins and then averaged. The error bars indicate the variance of the data in a given bin. The solid line is for the entire data set, the dotted line is for only the data at solar wind speeds greater than 500km/s and the dotted dashed line is for speeds less than 500km/s.

**Figure 7.** H<sup>+</sup> data in the same format as Figure 6.

**Figure 8.** O<sup>+</sup> (dashed) and H<sup>+</sup> (solid) perpendicular speed (a) and convection angle (b) a function of latitude. The data has been placed into latitude bins and averaged with the error bars indicating the variance in each bin.

**Figure 9.** In (a) the log of all the O<sup>+</sup> density data is shown as a function of the log of the solar wind dynamic pressure along with a linear fit.  $R$  is the correlation coefficient,  $R_{cl}$  is the ratio of the correlation coefficient to  $\frac{2}{\sqrt{N}}$ ,  $b$  is the y intercept, and  $m$  is the slope of the linear fit. (b) Shows the data placed into bins, and  $bsz$  is the bin size in units of the x-axis variable. (c) and (d) are in the same format as (b), but are sorted by IMF Bz where IMF Bz>0 is shown in (c) and IMF Bz<0 is shown in (d).

**Figure 10.** Log of the O<sup>+</sup> parallel flux versus the log of the solar wind dynamic pressure in the same format as Figure 9b.

**Figure 11.** Log of the O<sup>+</sup> density (a) and parallel flux (b) versus the solar wind speed times the magnitude of the IMF.

**Figure 12.** Log of the H<sup>+</sup> density (a) and parallel flux (b) versus IMF B<sub>y</sub>.

**Figure 13.** Log of the H<sup>+</sup> parallel speed(a) and O<sup>+</sup> parallel speed (b) versus IMF B<sub>y</sub>.

**Figure 14.** Log of the O<sup>+</sup> density (a) and parallel flux (b) versus IMF B<sub>y</sub>.

**Figure 15.** Log of the H<sup>+</sup> density (a) and parallel flux (b) versus the solar wind speed times the magnitude of the IMF. In panels c and d the data is sorted by IMF B<sub>z</sub> where IMF B<sub>z</sub>>0 is shown in c and IMF B<sub>z</sub><0 is shown in d.

Orbit	Kp For Orbit	Kp Daily	V <sub>sw</sub>
04/19/96 a	3+	4-	690
04/19/96 b	5-	4-	695
05/28/96	1-	1	360
06/14/96	1	1-	296
06/26/96	1	1	352
07/10/96	1-	0+	325
07/13/96	2	1+	390
07/24/95	1-	1-	345
07/26/96	2-	1+	385
07/29/96	1	1	375

**Table 1.** The Kp average for each orbit, the daily Kp average, and the average solar wind speed.

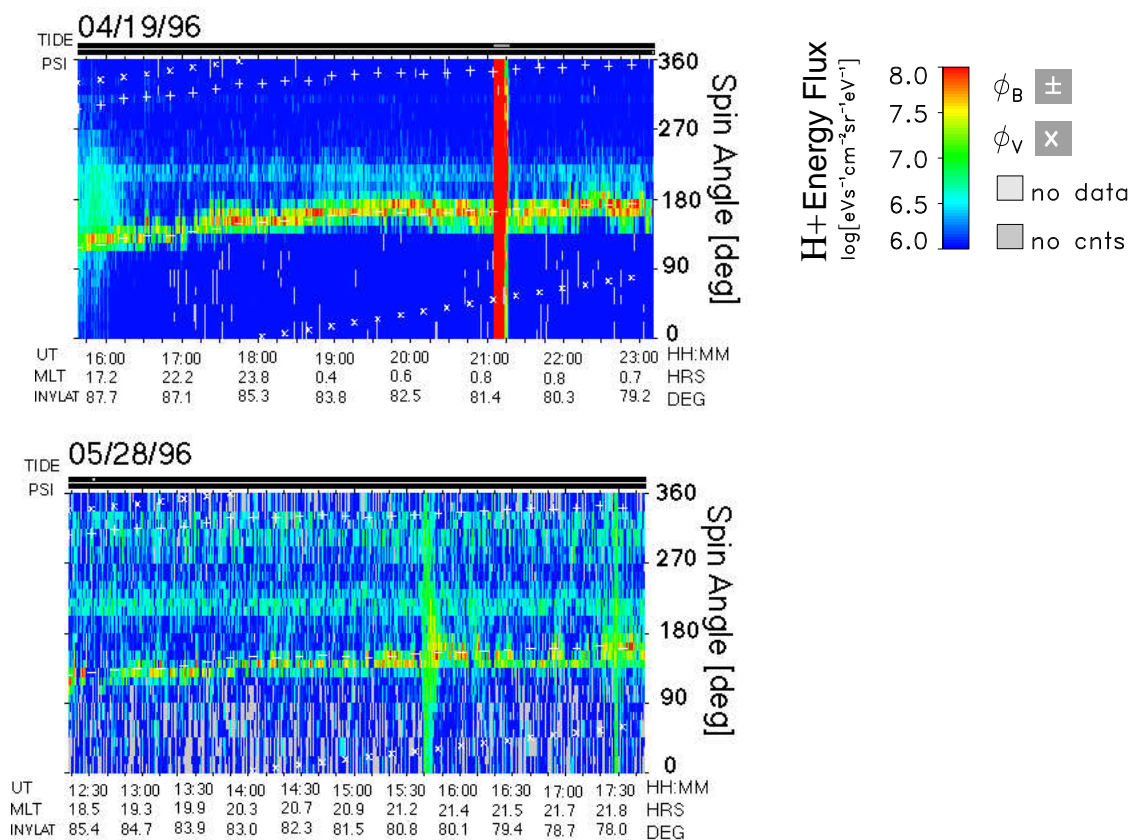


Figure 1

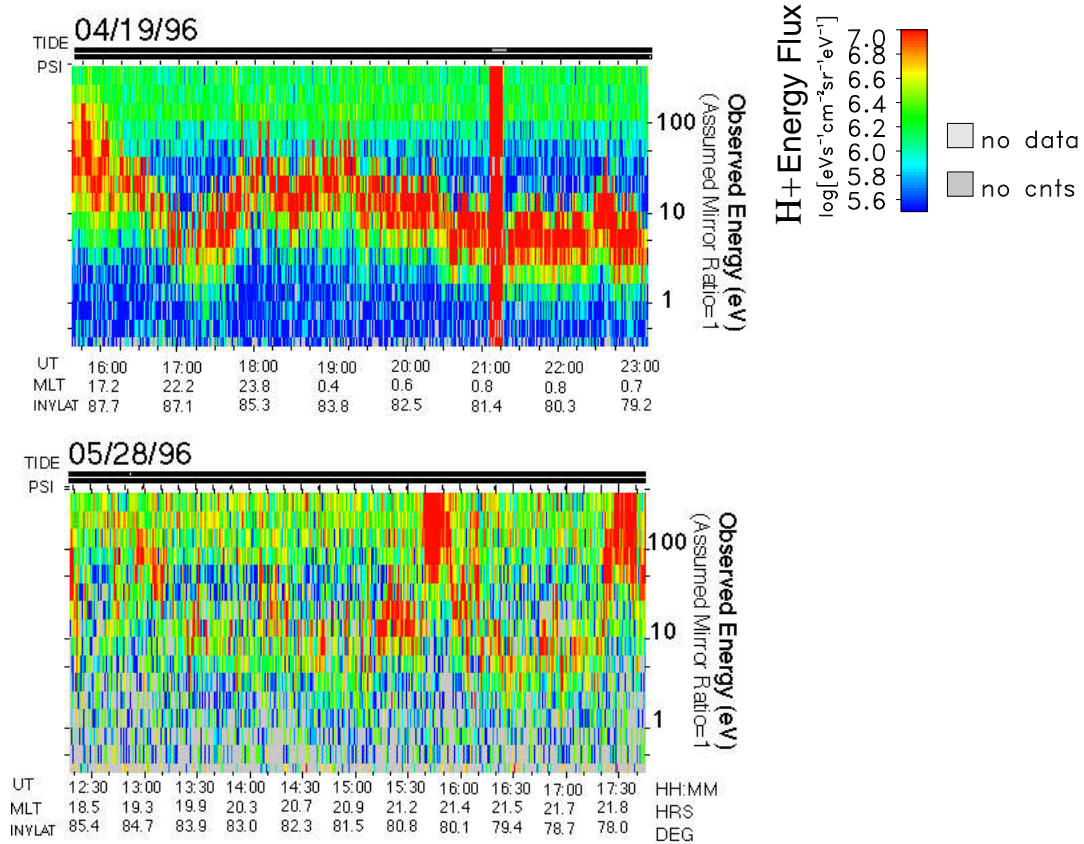


Figure 2

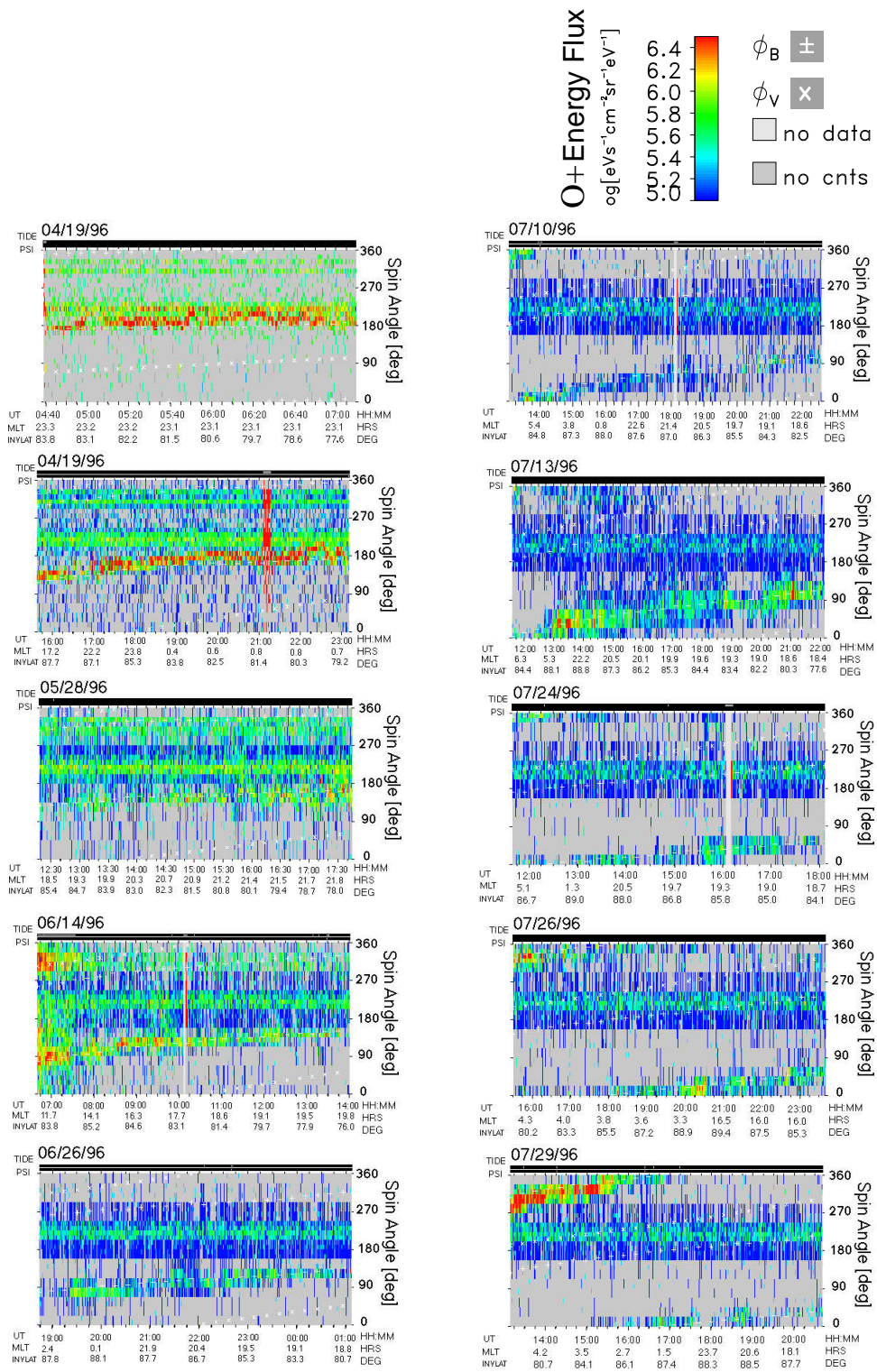
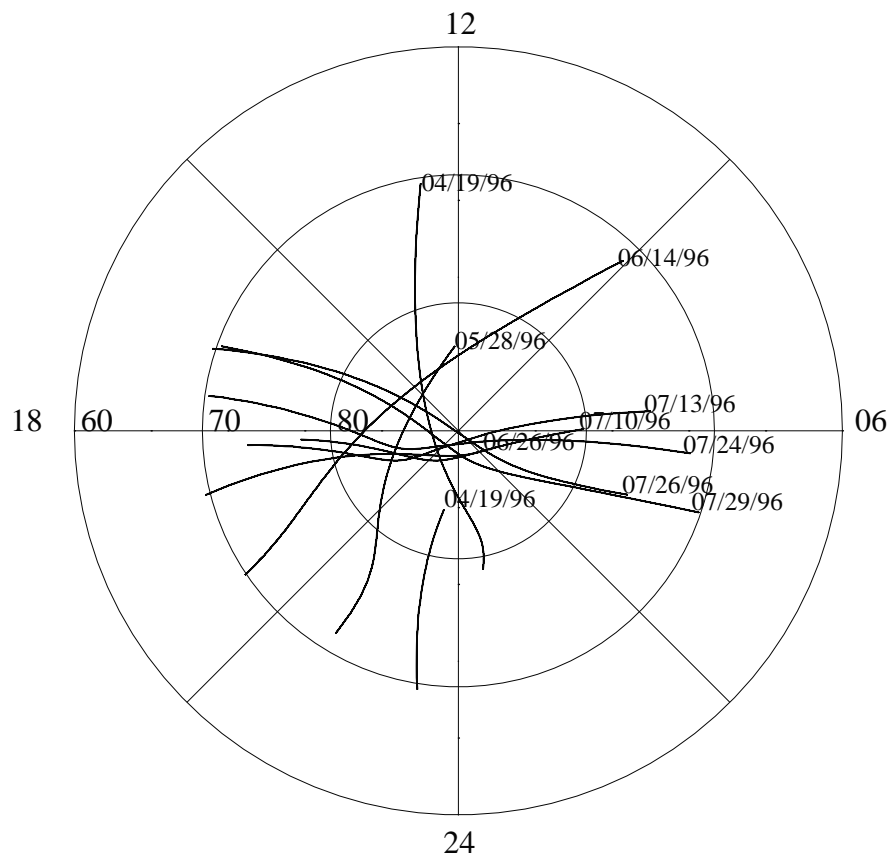


Figure 3

# POLAR Orbit Plots With PSI & TIDE Operating



Invariant Latitude (deg)

MLT (hrs)

Figure 4

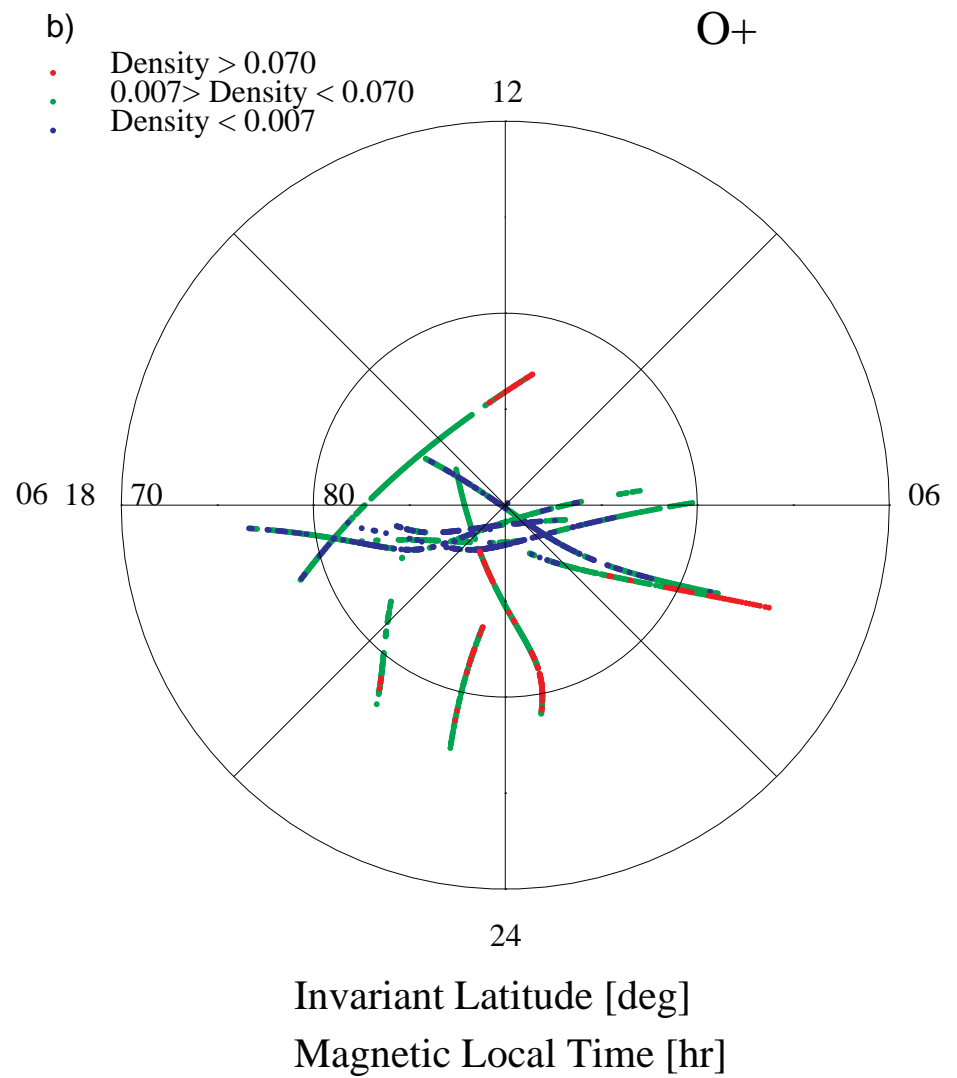
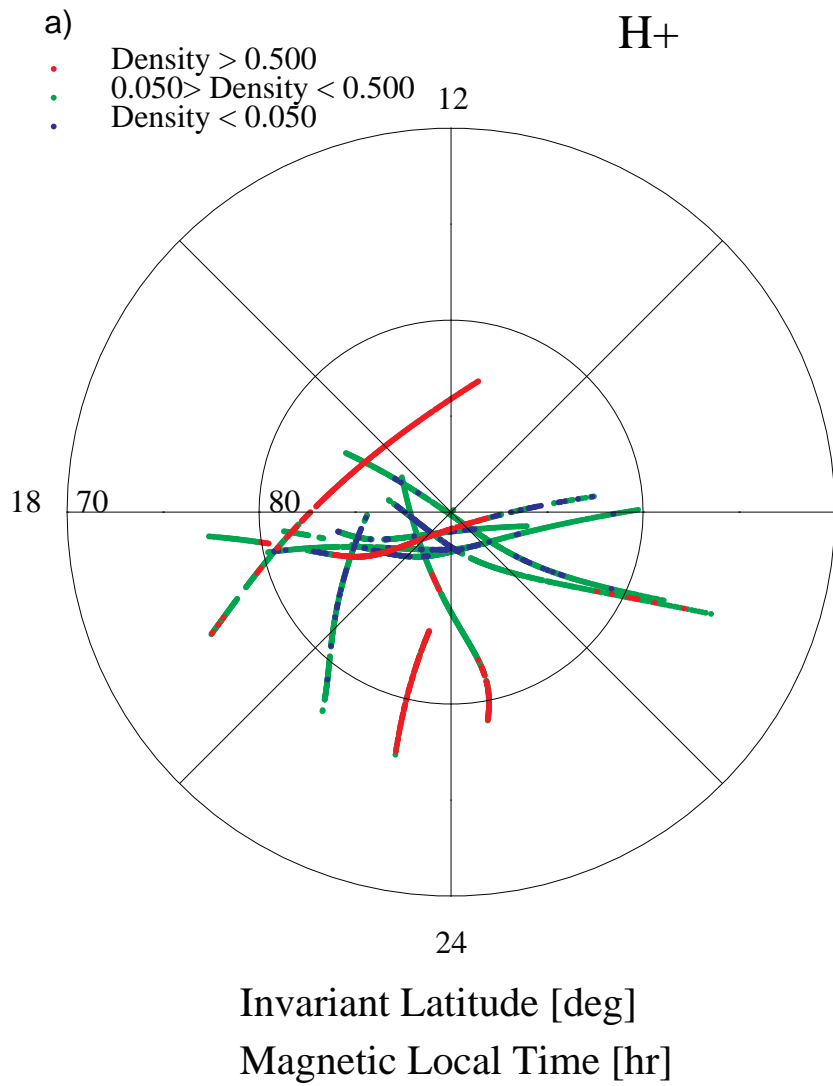


Figure 5

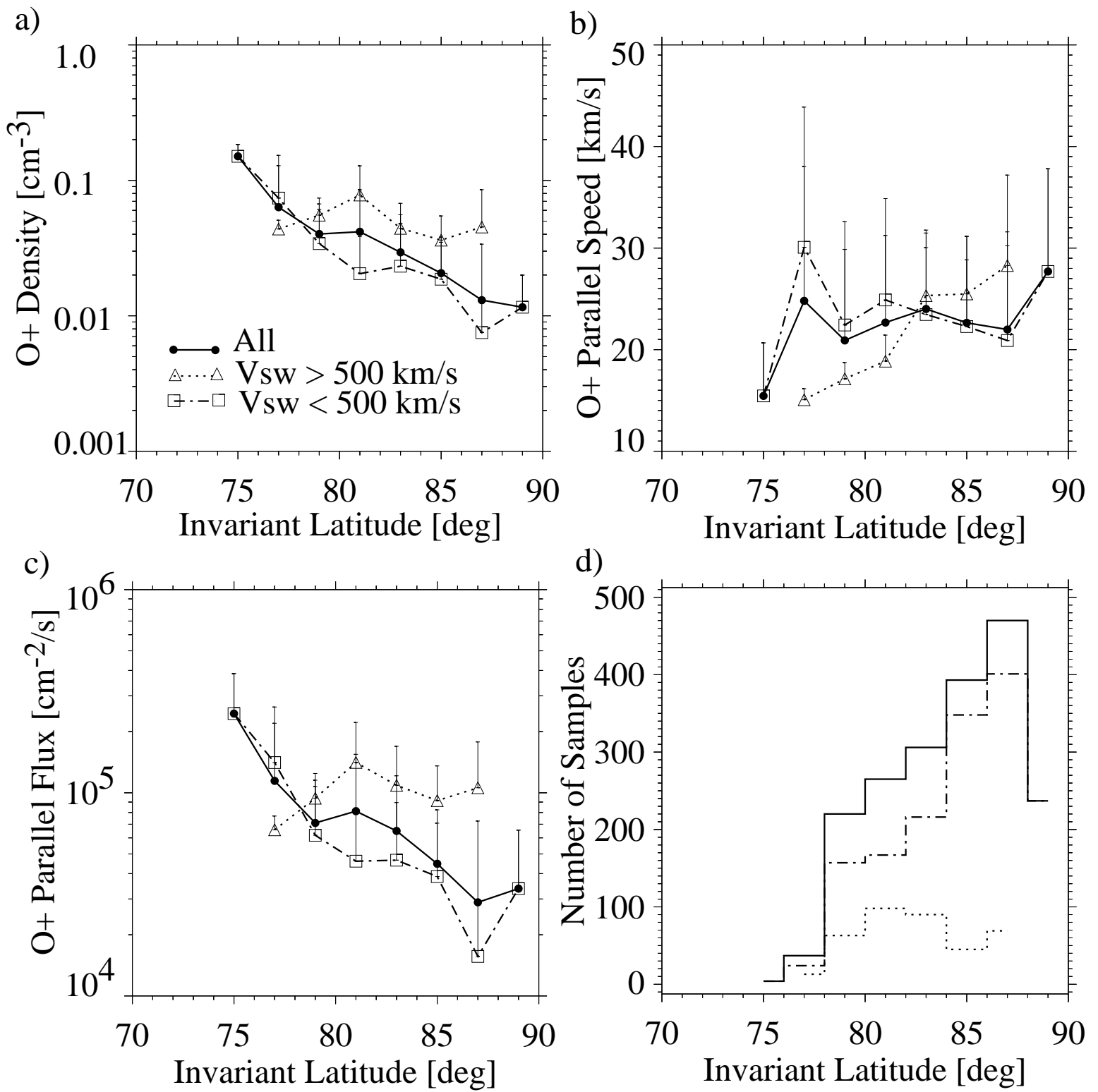


Figure 6

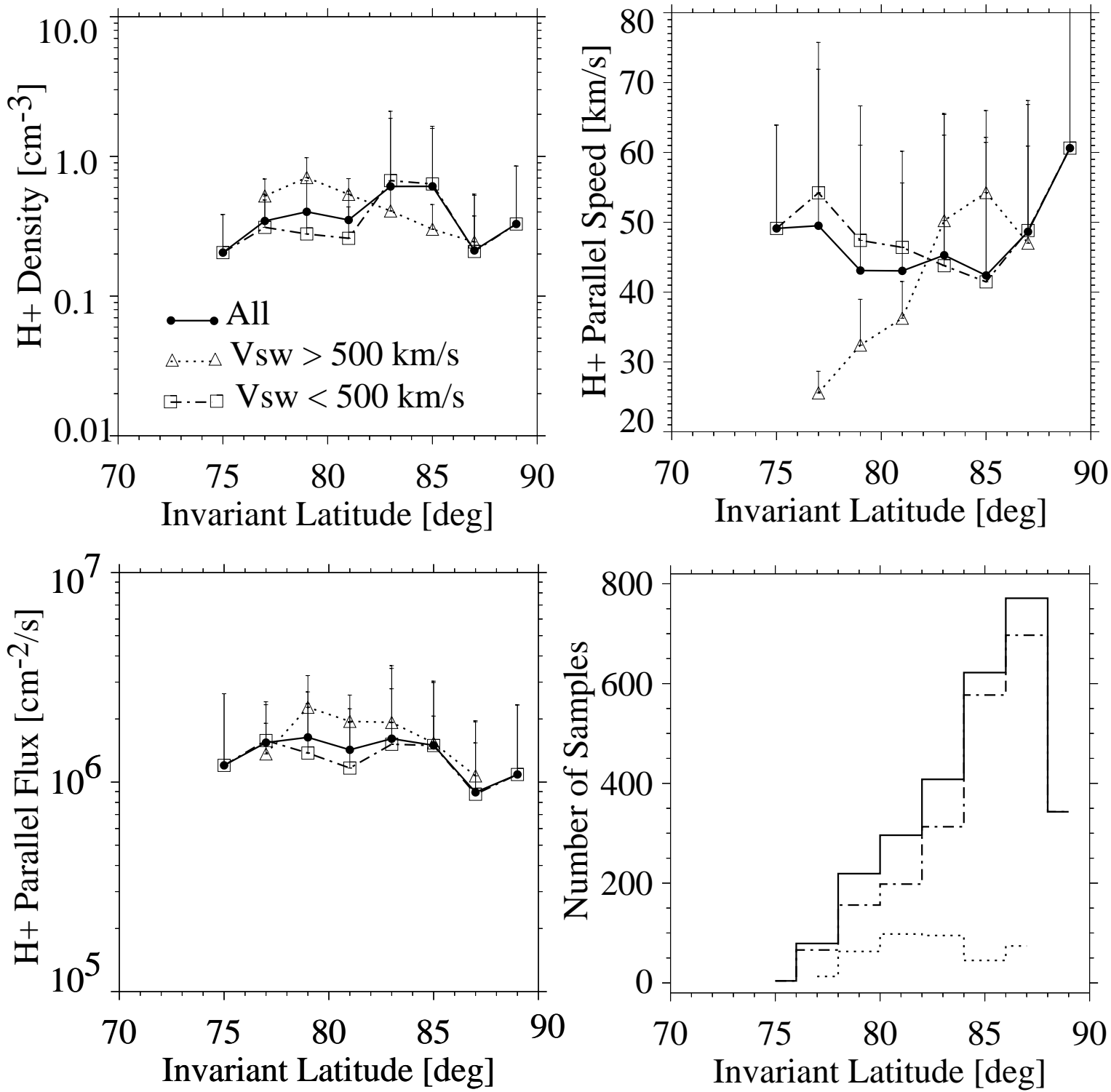


Figure 7

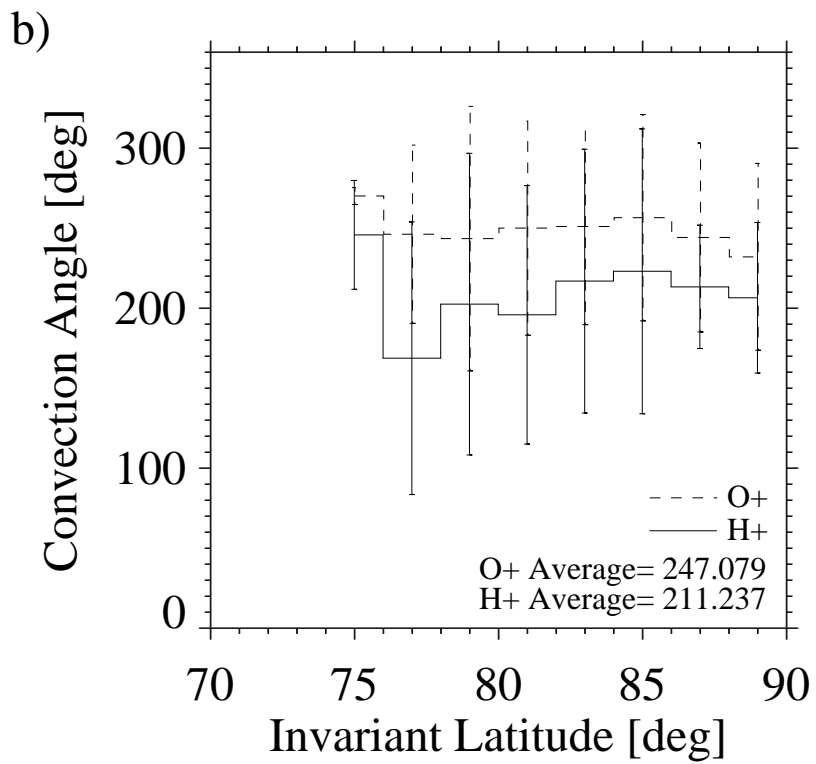
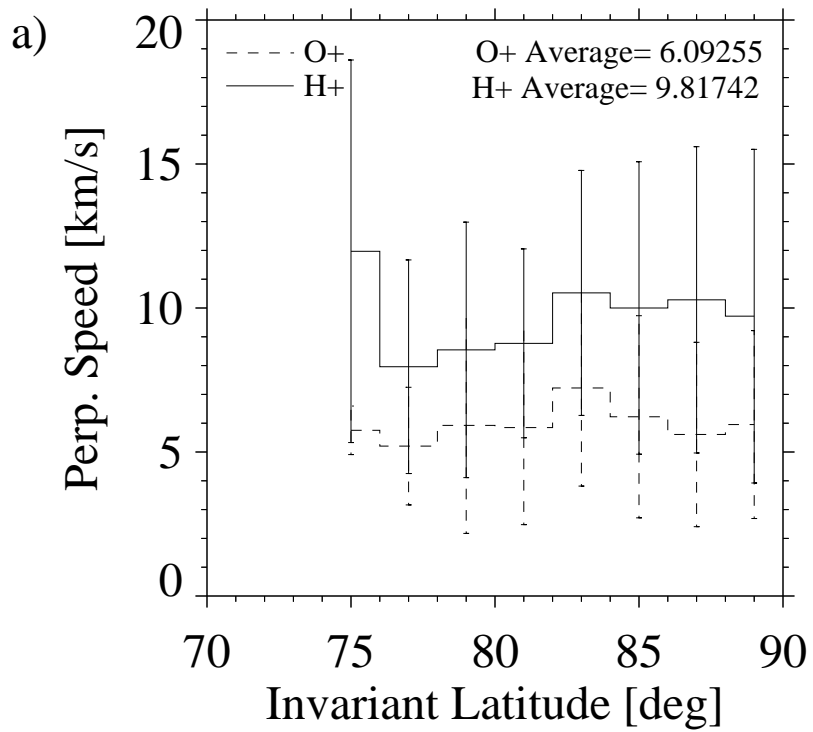


Figure 8

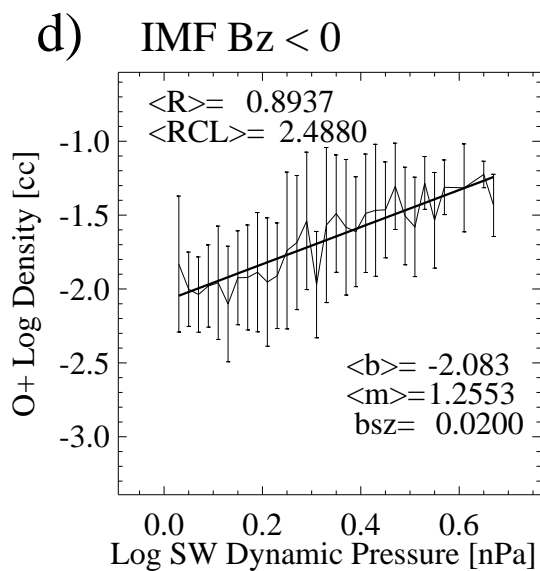
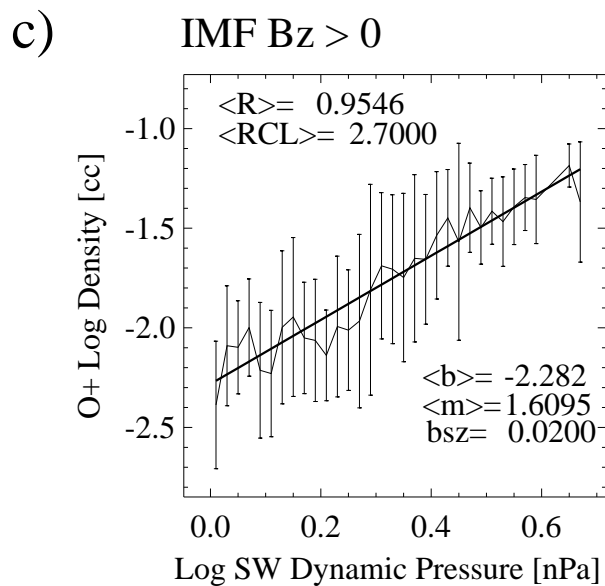
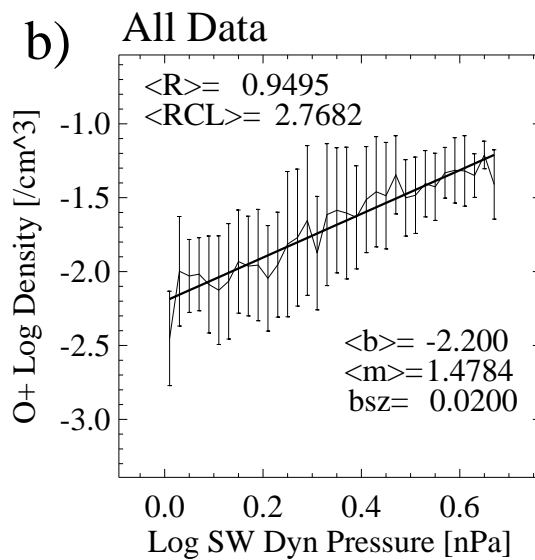
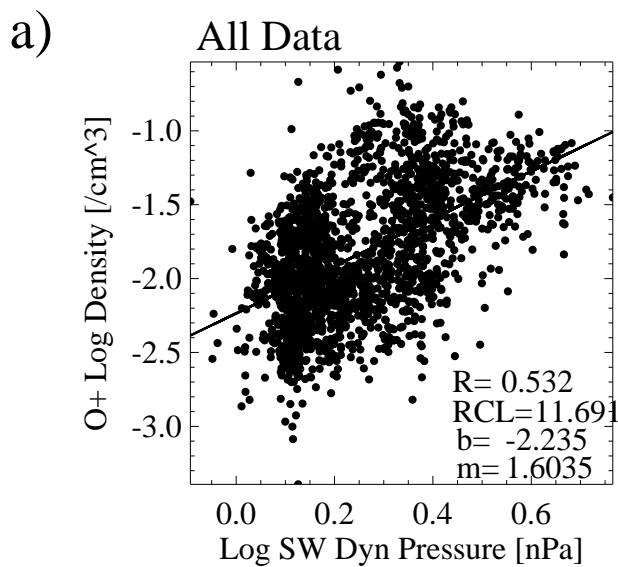


Figure 9

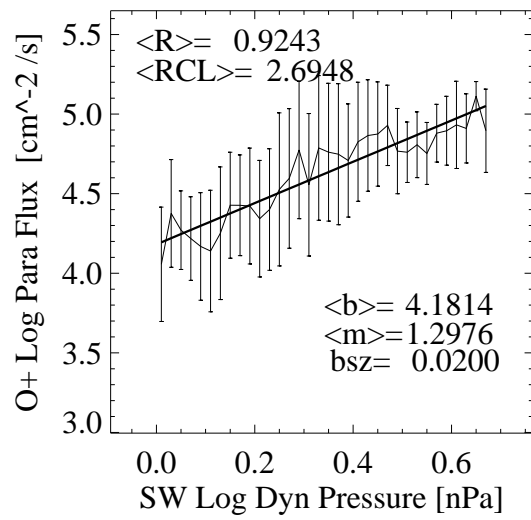


Figure 10

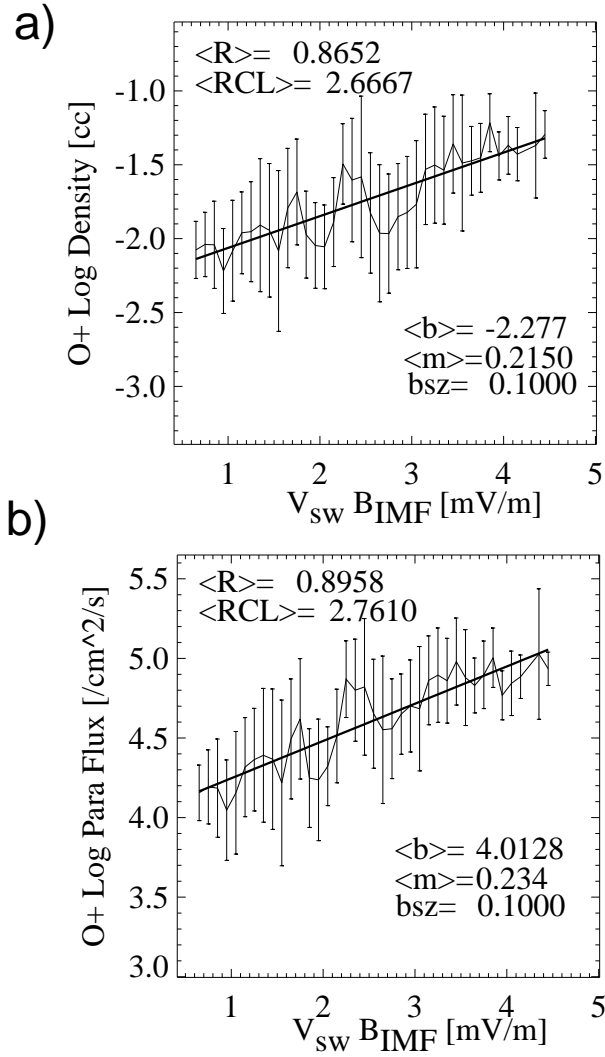


Figure 11

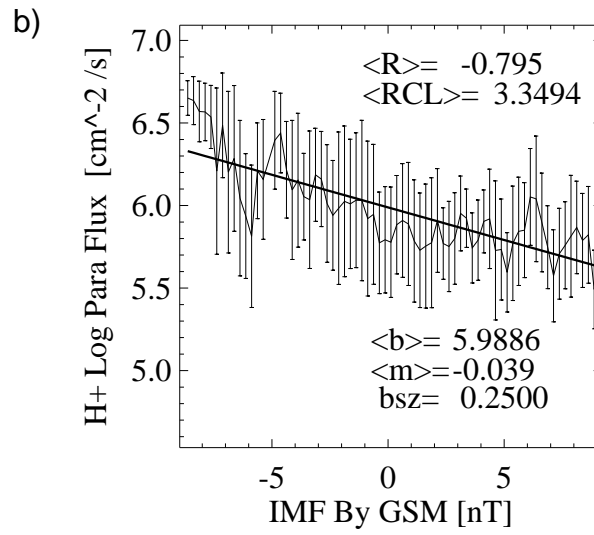
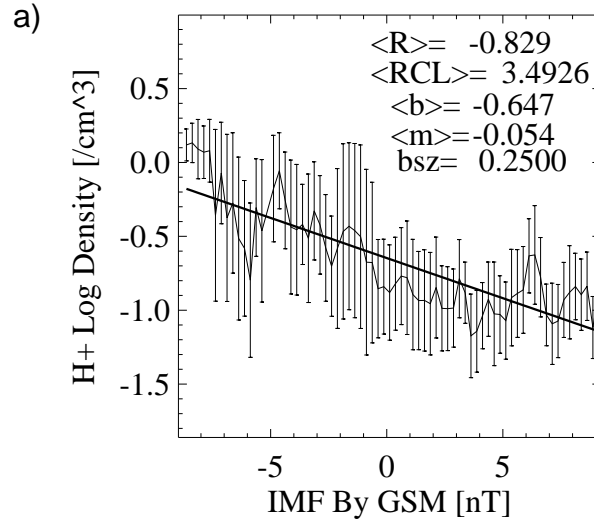


Figure 12

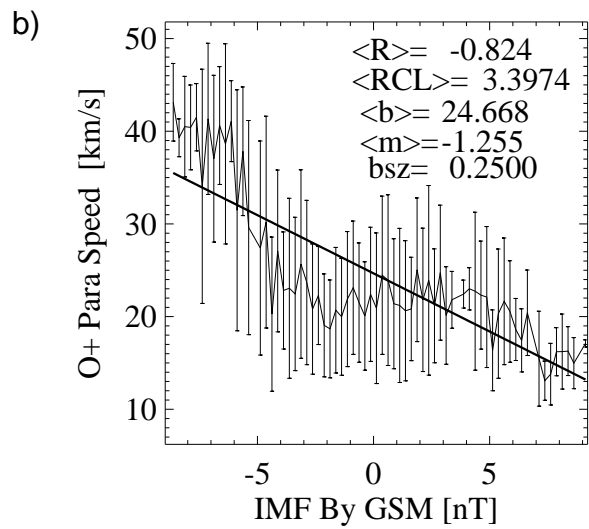
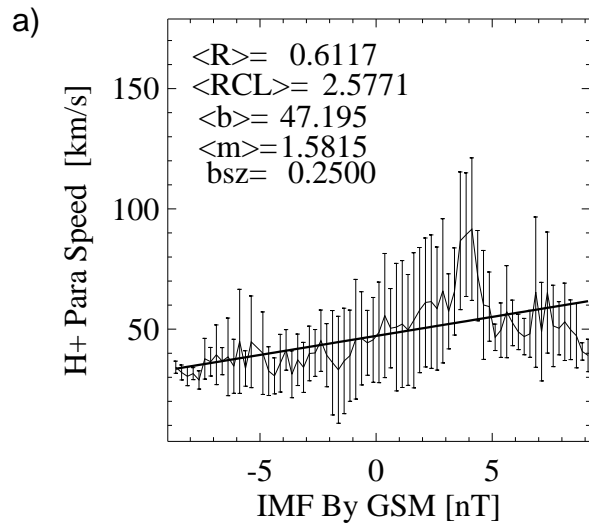


Figure 13

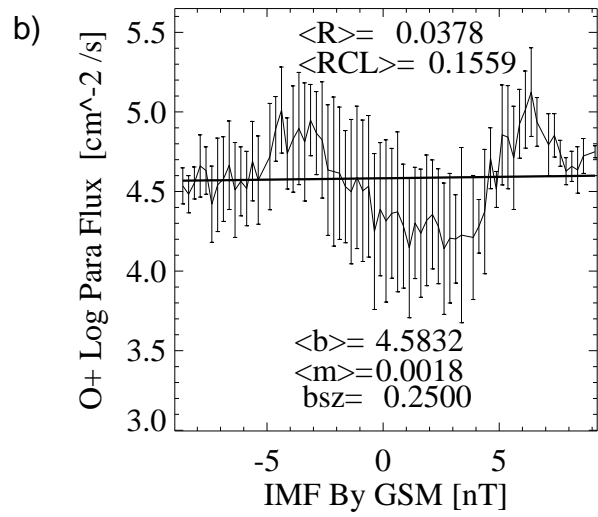
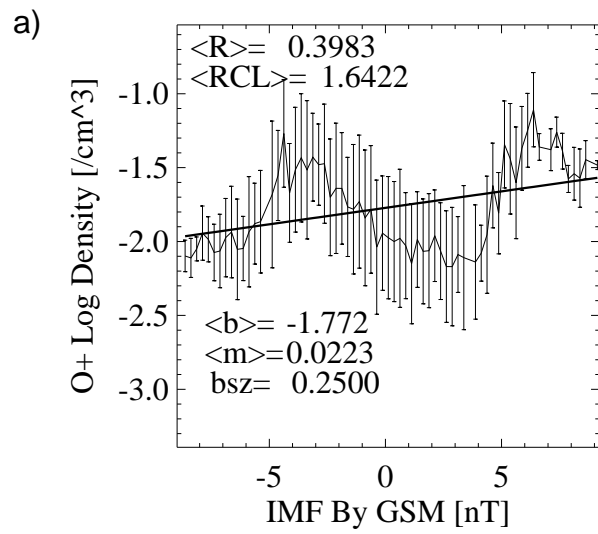


Figure 14

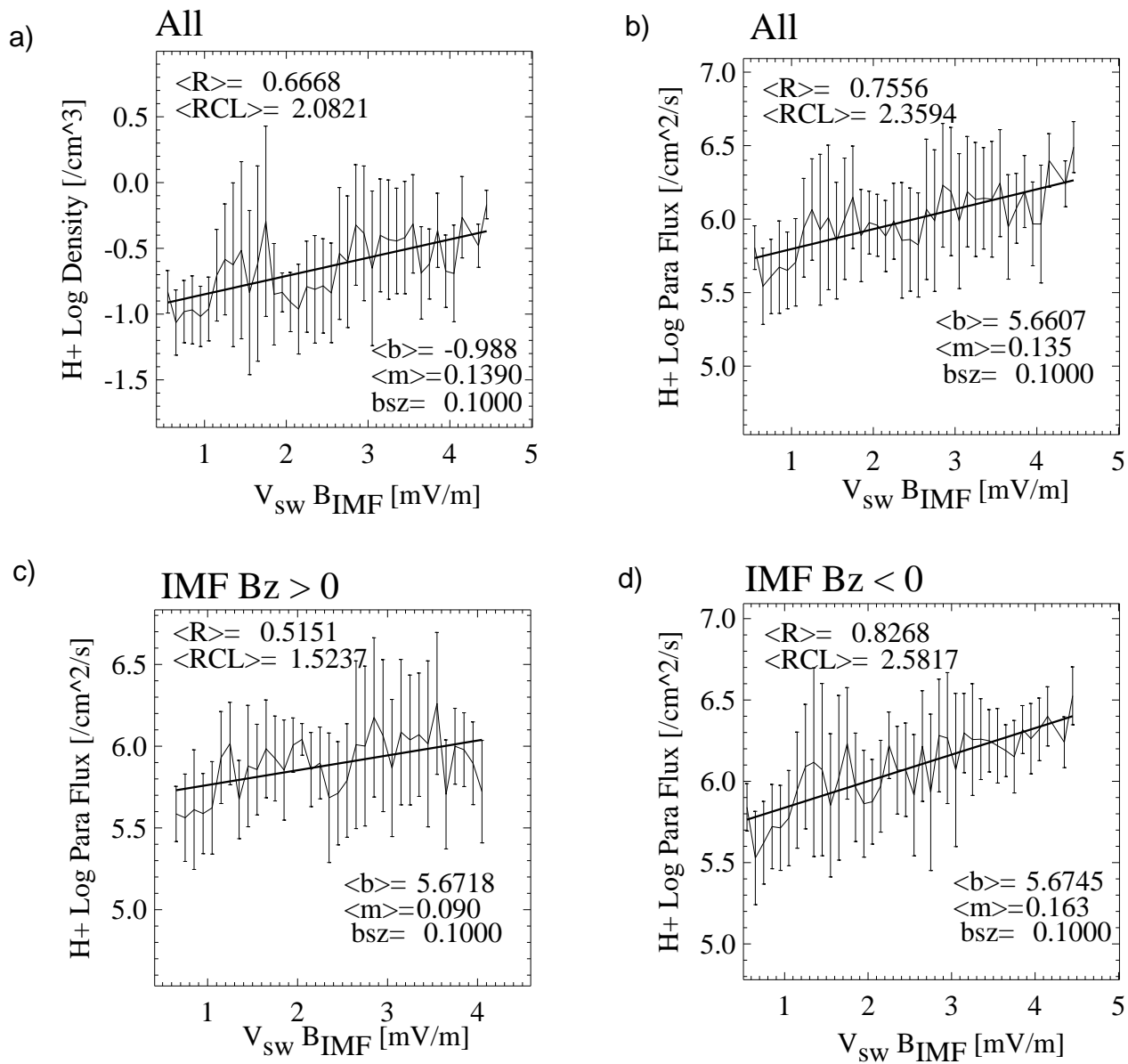


Figure 15